

國立交通大學

光電工程研究所

碩士論文

相位移長週期光纖光柵之設計及製作

Design and Fabrication of Phase-Sifted Long Period Fiber Gratings



研究生：張淑惠

指導教授：賴暎杰 博士

中華民國九十四年七月

相位移長週期光纖光柵之設計及製作

Design and Fabrication of Phase-Sifted Long Period Fiber Gratings

研究生:張淑惠

Student: Shu-Hui Chang

指導教授:賴暎杰 博士

Advisor: Dr. Yinchieh Lai

國立交通大學

光電工程研究所



碩士論文

A Thesis

Submitted to Department of Photonics & Institute of Electro-Optical Engineering

College of Electrical Engineering and Computer Science

National Chiao Tung University

In Partial Fulfillment of Requirements for the Degree of

Master in Electro-Optical Engineering

July 2005

Hsinchu, Taiwan, Republic of China

中華民國九十四年七月


相位移長週期光纖光柵之設計及製作

研究生:張淑惠

指導教授:賴暎杰 博士

國立交通大學光電工程研究所碩士班

摘要



在本論文中，我們研究如何由理論配合實驗去設計及製作相位移長週期光纖光柵。在實驗上，我們用紫外光逐點曝照光纖的方式，使其產生週期性的折射率改變。藉由控制不同的曝照時間，可製作出各種不同折射率變化的均勻長週期光纖光柵。由所得到的均勻長週期光纖光柵的頻譜，再配合模態耦合理論，可推得折射率變化與時間的關係和折射率對波長的變化率與波長的關係。

利用所得到的參數，我們使用演化演算法來設計最佳化長週期光纖光柵的耦合係數函數，並藉由控制不同的曝照時間和每段均勻光纖光柵之間的相位移，來試製複雜且能實際應用於光纖通訊中的平坦化長週期光纖光柵濾波器。

Design and Fabrication of Phase-Sifted Long Period Fiber Gratings

Student: Shu-Hui Chang

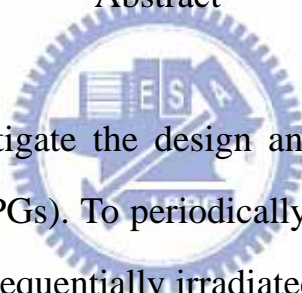
Advisor: Dr. Yinchieh Lai

Department of Photonics & Institute of Electro-Optical Engineering

College of Electrical Engineering and Computer Science

National Chiao Tung University

Abstract

The logo of National Chiao Tung University is a circular emblem with a gear-like border. Inside the circle, there are stylized representations of a book, a building, and a person, with the letters 'ES' and 'A' prominently displayed.

In this thesis, we investigate the design and fabrication of phase-shifted long-period fiber gratings (LPGs). To periodically modulate the refractive index of the fiber core, the fiber is sequentially irradiated point-by-point by a UV laser beam. The refractive index change of fabricated long-period fiber gratings can be changed by adjusting the UV exposure time. Using the coupled-mode theory to analyze the measured data, we calibrate the relationship of the fiber core refractive index change with the wavelength as well as with the exposure time. With the calibration parameters, an Evolutionary Programming (EP) algorithm is then used to design a flat-band LPGs by optimizing the coupling coefficient distribution function. By controlling the UV exposure time and the phase shifts between each uniform LPGs, complex LPGs with advanced characteristics can be fabricated.

Acknowledge

在交大的這兩年來，受到許多人的幫忙，心中有無限的感謝。

賴暎杰老師的學富五車且個性溫和，不論學業上、研究上和生活中都給予我許多的關懷和幫助。在這裡特別感謝莊凱評學長、許立根博士、李澄鈴學姊和徐桂珠學姊。莊凱評學長在我碩一的那一年，很盡力的將他在光纖光學實驗室裡面的一切教導給我，使我很快的就進入了狀況。許立根學長在我研究的過程中不斷的給我建議，提供我思考方向及儀器的協助。李澄鈴學姊給我一些模擬的程式，使我在模擬時能有所依據。徐桂珠學姊則是在我生活上及研究上，不斷的給我建議及照顧，從學姊那裡真的學到很多東西。另外感謝陳南光學長，提供一些實驗儀器的協助。還有和我一同畢業的倩仔、金水和銘峰，學弟人豪及鐘响，有了你們的陪伴，在交大的這兩年真是過的多姿多采。

最後感謝支持我的家人和一些朋友，讓我心情低落的時候，有個溫暖的避風港，想大吼大叫的時候，有個對象。總之，謝謝你們接收了我所有的情緒，一路陪伴我。



Contents

Chinese Abstract	i
English Abstract.....	ii
Acknowledgement.....	iii
Contents.....	iv
List of Figures.....	vi
Chapter 1. Introduction.....	1
1.1 Introduction of Fiber Gratings.....	1
1.2 Motivation of the Research.....	4
1.3 Structure of this Thesis.....	4
Chapter 2. Synthesis of Long-Period Fiber Gratings.....	8
2.1 Coupled-Mode Theory.....	8
2.2 Transfer Matrix Method.....	10
2.3 Evolutionary Programming Algorithm.....	11
2.3.1 Long-Period Fiber Gratings Synthesis Using Evolutionary Programming.....	11
2.3.2 Simulation of Flat-Band Long-Period Fiber Gratings.....	14
Chapter 3. Experimental Setup and Results.....	20
3.1 Experimental Setup.....	20
3.2 Calibration of the Parameters.....	21
3.3 Simulation and Experimental Results.....	23
3.3.1 Uniform Long-Period Fiber Gratings.....	23
3.3.2 Simple Phase-Shifted Long-Period Fiber Gratings.....	24
3.3.3 Flat-Band Long-Period Fiber Gratings.....	24

Chapter 4. Conclusion and Future Work.....44

 4.1 Conclusion.....44

 4.2 Future Work.....45

References.....46



List of Figures

Fig. 1.1	: Two coherent UV beams produce an interference pattern in the fiber.....	5
Fig. 1.2	: The fiber grating is fabricated by a UV beam incident to a phase mask.....	6
Fig. 1.3	: Diffraction of light by a grating.....	7
Fig. 2.1	: Flow chart of the proposed EP algorithm for LPG design.....	16
Fig. 2.2	: Target and designed transmission spectra of the flat-band LPG.....	17
Fig. 2.3	: Designed amplitude of the coupling coefficient distribution function for the flat-band LPG.....	18
Fig. 2.4	: Designed phase of the coupling coefficient distribution function for the flat-band LPG.....	19
Fig. 3.1	: Experimental setup of sequential point writing.....	27
Fig. 3.2	: Transmission spectra for LPGs with different grating periods (450 μm and 430 μm).....	28
Fig. 3.3	: Transmission spectra for LPGs with different grating periods (430 μm and 420 μm).....	28
Fig. 3.4	: Transmission spectra for LPGs with different grating periods (420 μm and 350 μm).....	29
Fig. 3.5	: Transmission spectra for LPGs with different grating periods (350 μm and 210 μm).....	29

Fig. 3.6	:	The core refractive index change versus wavelength.....	30
Fig. 3.7	:	The modulated refractive index change versus time.....	30
Fig. 3.8	:	Transmission spectra for uniform LPG (exposure time = 1s).....	31
Fig. 3.9	:	Transmission spectra for uniform LPG (exposure time = 2s).....	31
Fig. 3.10	:	Transmission spectra for uniform LPG (exposure time = 3s).....	32
Fig. 3.11	:	Transmission spectra for uniform LPG (exposure time = 4s).....	32
Fig. 3.12	:	Transmission spectra for uniform LPG (exposure time = 6s).....	33
Fig. 3.13	:	Transmission spectra for uniform LPG (exposure time = 8s).....	33
Fig. 3.14	:	Transmission spectra for uniform LPG (exposure time = 10s).....	34
Fig. 3.15	:	Single phase-shifted LPG.....	35
Fig. 3.16	:	Double phase-shifted LPG.....	35
Fig. 3.17	:	Multi-phase-shifted LPG.....	35
Fig. 3.18	:	Transmission spectra for single phase-shifted LPG ($L_1 = L_2 = 19.5mm, \phi = \pi / 2$).....	36
Fig. 3.19	:	Transmission spectra for single phase-shifted LPG ($L_1 = L_2 = 19.5mm, \phi = \pi$).....	36
Fig. 3.20	:	Transmission spectra for double phase-shifted LPG ($L_1 = L_2 = L_3 = 15.6mm, \phi_1 = \phi_2 = \pi$).....	37
Fig. 3.21	:	Transmission spectra for double phase-shifted LPG	

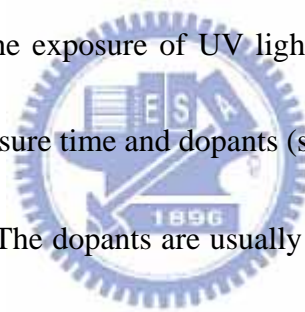
	$(L_1 = L_2 = L_3 = 15.6mm, \phi_1 = \pi/2, \phi_2 = \pi)$	38
Fig. 3.22 :	Transmission spectra for multi-phase-shifted LPG (120 periods, 6 sections, every section 20 periods, 3s).....	39
Fig. 3.23 :	Transmission spectra for multi-phase-shifted LPG (120 periods, 3 sections, every section 40 periods, 3s).....	40
Fig. 3.24 :	Transmission spectra for the flat-band LPG.....	41
Fig. 3.25 :	The simulated spectra with different ratios of the coupling coefficient distribution functions compared to the original one. (a) The ratio is less than one. (b) The ratio is larger than one.	42
Fig. 3.26 :	The simulated spectra at different fringe visibility of index change compared to the original one. (a) The fringe visibility of index change is less than the simulated one; (b) larger than the simulated one.	43



Chapter 1. Introduction

1.1 Introduction of Fiber Gratings

Fiber gratings are fiber devices that have found many applications in optical communication and optical sensing. They are produced by exposing an optical fiber to ultra-violet (UV) lights that perturb the refractive index of the core to form a periodic index modulation profile. The photosensitive phenomenon in optical fibers was first demonstrated by Hill et al. in 1978 [1]. Here photosensitivity means that the refractive index of certain doped glasses can be raised by the exposure of UV lights. The magnitude of the refractive index change depends on the exposure time and dopants (such as Germania) in the fiber and is typically between 10^{-6} to 10^{-3} . The dopants are usually doped only in the core of fibers, so the UV induced index change is only in the core, not in the cladding of fibers. By using the techniques such as hydrogen loading, an index change as high as 10^{-2} can be obtained. Fiber gratings are usually fabricated by a variant of the transverse holographic method first proposed by Meltz et al. [2] in 1989. The UV interference pattern is imposed on the fiber from the side as shown in Fig. 1.1. After a few years the phase mask technique [3-5] as shown in Fig. 1.2 becomes widely used to simplify the fabricated procedure and yet produce fiber gratings with high performance. In order to fabricate long and complex fiber grating with advance characteristics, the systems of sequential writing have also been proposed and



demonstrated [6-8].

To fabricate fiber gratings for various applications, it is important to have tools to analyze and synthesize them according to the application purposes. The most common mathematical model used to describe wave propagation in a fiber grating is the coupled-mode equation [9]. Together with the inverse algorithms such as Gel'fand-Levitan-Marchenko (GLM) inverse-scattering method [10-11], Layer-Peeling (LP) inverse-scattering algorithms [12-14] and Evolutionary Algorithm (EA) [15-17] including Genetic Algorithm (GA) and Evolutionary programming (EP) algorithm, complicated fiber gratings can be inversely designed.



A fiber grating is simply an optical diffraction grating as shown in Fig. 1.3, and thus its effect upon a light-wave incident into the grating at an angle θ_1 can be described by the grating equation

$$n \sin \theta_2 = n \sin \theta_1 + m \frac{\lambda}{\Lambda} \quad (1.1)$$

where θ_2 is the angle of the diffracted wave and the integer m determines the diffraction order. This equation predicts not only the directions θ_2 into which constructive interference occurs, but also is capable of determining the wavelength at which a fiber grating can most efficiently couple lights between the two modes.

Fiber gratings can be broadly classified into two types: Bragg gratings (also called reflection and short-period gratings), in which the coupling occurs between modes traveling in

opposite directions; and transmission gratings (also called long-period gratings), in which the coupling is between modes traveling in the same direction. Since the mode propagation constant β is simply $\beta = (2\pi/\lambda)n_{eff}$ where $n_{eff} = n_{co} \sin \theta$, we may rewrite for guided modes as

$$\beta_2 = \beta_1 + m \frac{2\pi}{\Lambda} \quad (1.2)$$

For first-order reflective diffraction, which usually dominates in a fiber Bragg grating, $m=-1$. Positive and negative β values describe modes that propagate in the $+z$ and $-z$ direction, respectively. By using (1.2) and recognizing $\beta_2 < 0$, we find that the resonant

wavelength for the reflection of a mode of index $n_{eff,1}$ into a mode of index $n_{eff,2}$ is

$$\lambda = (n_{eff,1} + n_{eff,2})\Lambda. \quad (1.3)$$

If the two modes are identical, we get the familiar result for Bragg reflection: $\lambda = 2n_{eff}\Lambda$.

When light is diffracted by a transmission grating, the first mode is a core mode while the second one is a cladding mode. Since here $\beta_2 > 0$, the resonant wavelength for a transmission grating is

$$\lambda = (n_{eff,1} - n_{eff,2})\Lambda. \quad (1.4)$$

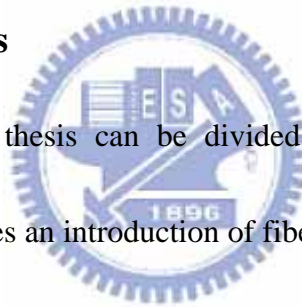
For co-propagating coupling at a given wavelength, evidently a much longer grating period Λ is required for counter-propagating coupling.

1.2 Motivation of the Research

Long-period fiber gratings (LPGs) can be designed to have a variety of profiles depending on its applications, such as band-rejection filters [18], high sensitivity sensors [19], mode converters [20], and erbium-doped fiber amplifier gain flattening filters [21]. Our group has presented a novel LPGs synthesis method using a revised EP algorithm [17]. We believe that using the EP algorithm is an effective and practical way for optimally designing complicated LPGs.

1.3 Structure of this Thesis

The main structure of this thesis can be divided into four parts. Chapter 1 is an introductory chapter which includes an introduction of fiber gratings and the motivation of the research. Chapter 2 describes the synthesis of long-period fiber gratings, which include the coupled-mode theory, transfer matrix method and evolution programming algorithm. Chapter 3 presents the experimental setup and results of fabricating phase-shifted long-period fiber gratings. In Chapter 4, we give a brief conclusion and provide directions of the further research related to this topic.



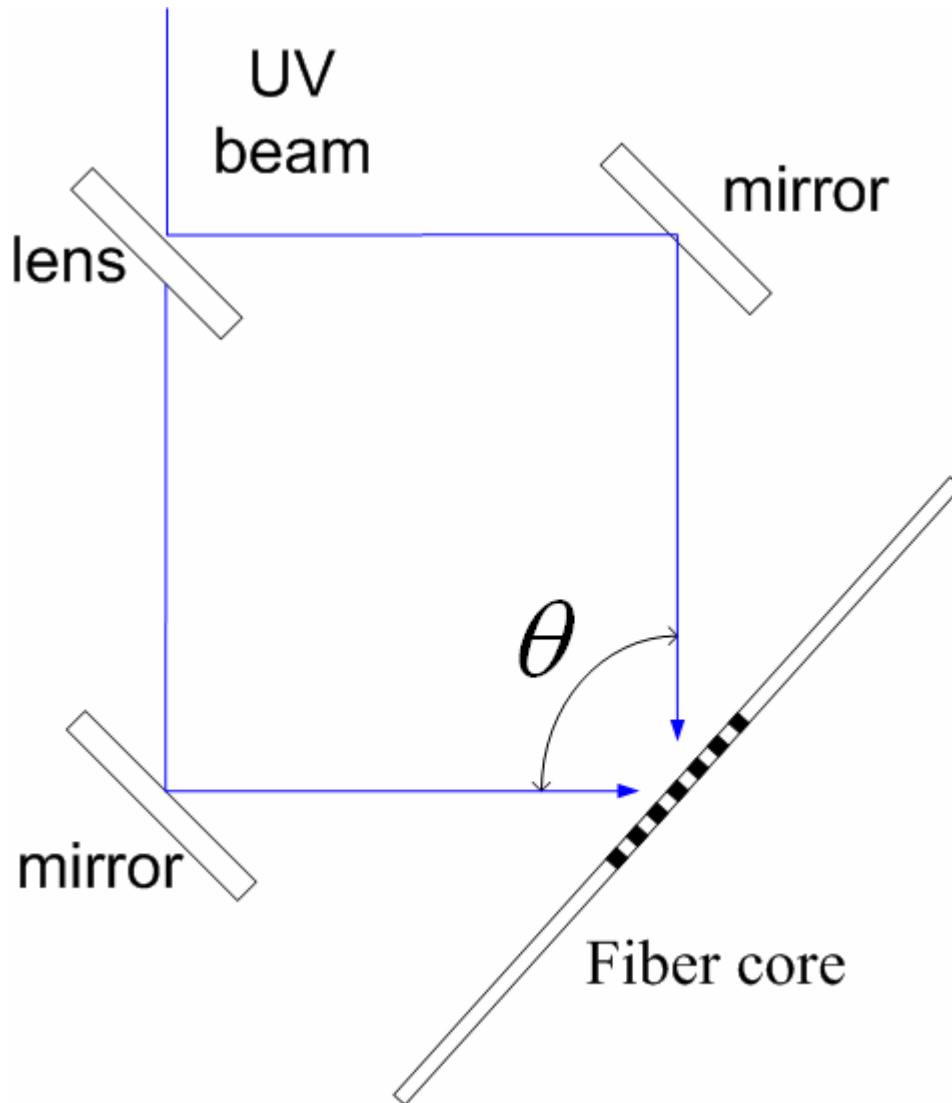


Fig. 1.1 Two coherent UV beams produce an interference pattern in the fiber. The period of the grating depends on the angle θ of the two incident beams.

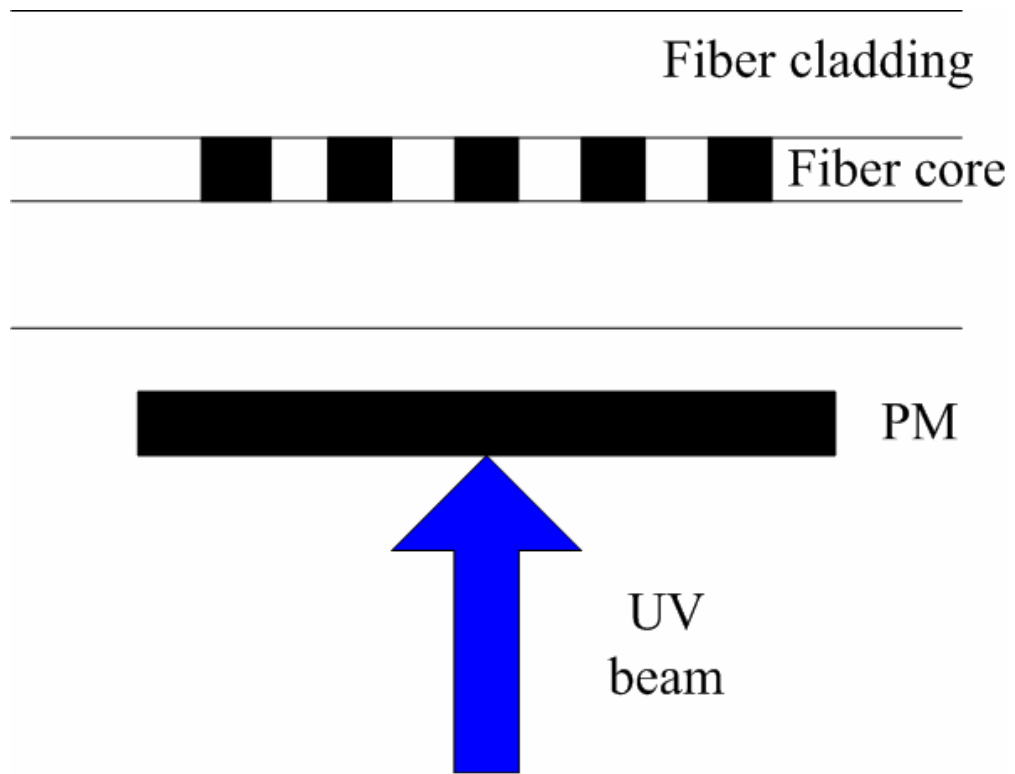


Fig. 1.2 The fiber grating is fabricated by a UV beam incident to a phase mask (PM). The period of the fiber grating is half of the PM period.

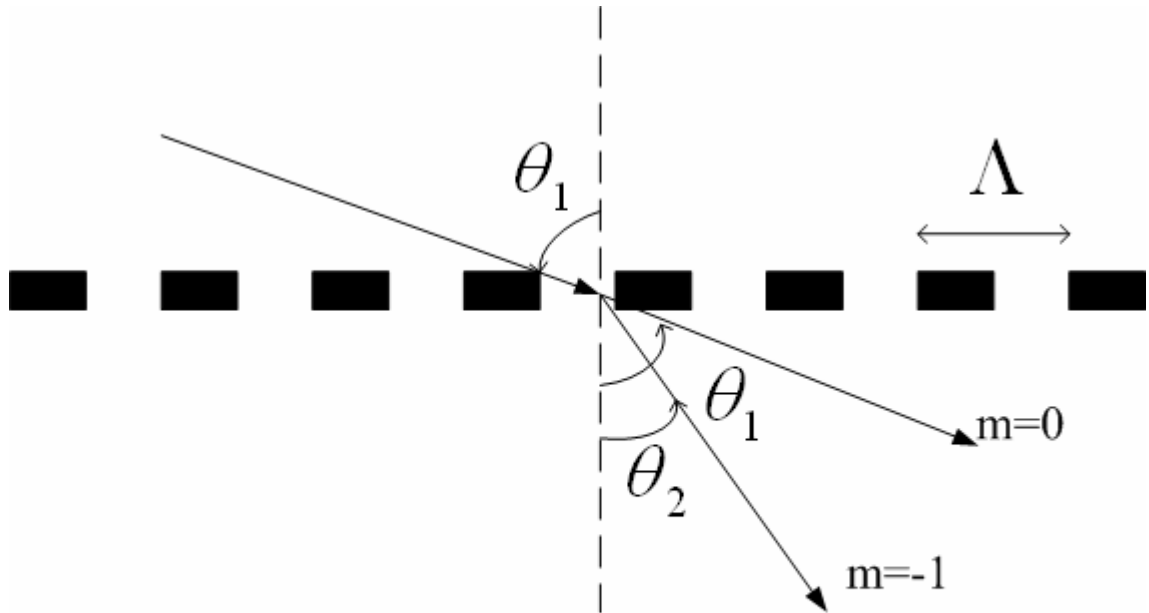


Fig. 1.3 Diffraction of light by a grating

Chapter 2. Synthesis of Long-Period Fiber Gratings

In this chapter we will explain the modeling and synthesis of long-period fiber gratings.

In the following derivation, for simplicity a perturbation to the core refractive index n_{co} will

be described by [9]

$$\Delta n_{co}(z) = \overline{\Delta n_{co}}(z) \left\{ 1 + \nu \cos \left[\frac{2\pi}{\Lambda} z + \phi(z) \right] \right\} \quad (2.1)$$

where $\overline{\Delta n_{co}}(z)$ is the dc index change spatially averaged over a grating period, ν is the fringe visibility of the index change, Λ is the period, and $\phi(z)$ describes the grating phase.



2.1 Coupled-Mode Theory

Since the long-period fiber grating couples the forward propagating guided core mode of amplitude $A_1(z)$ to one of the co-propagating cladding modes of amplitude $A_2(z)$, the coupled-mode equations of long-period fiber grating can be written as

$$\frac{dA^{co}(z)}{dz} = i\hat{\sigma} A^{co}(z) + i\kappa(z)A^{cl}(z) \quad (2.2)$$

$$\frac{dA^{cl}(z)}{dz} = -i\hat{\sigma} A^{cl}(z) + i\kappa^*(z)A^{co}(z) \quad (2.3)$$

where the amplitudes A^{co} and A^{cl} are $A^{co}(z) \equiv A_1(z) \exp[-i(\sigma_{11} + \sigma_{22})z/2] \exp(i\delta z - \phi/2)$

and $A^{cl}(z) \equiv A_2(z) \exp[-i(\sigma_{11} + \sigma_{22})z/2] \exp(-i\delta z + \phi/2)$, and σ_{11} , σ_{22} are dc coupling

coefficients defined in (2.4).

$$\sigma_{kj}(z) = \frac{\omega n_{co}}{2} \overline{\Delta n_{co}}(z) \iint_{core} dx dy \vec{e}_{kt}(x, y) \cdot \vec{e}_{jt}^*(x, y) \quad (2.4)$$

The mode coupling coefficient functions are defined as

$$\kappa_{kj}(z) = \frac{V}{2} \sigma_{kj}(z) \quad (2.5)$$

$$k, j = 1, 2$$

where $\bar{e}_{ji}(x, y)$ are the transverse mode fields. When j is equal to 1, it refers to the core mode. When j is equal to 2, it describes the cladding mode.

In (2.2) and (2.3), $\kappa = \kappa_{21} = \kappa_{12}^*$ is the ac cross-coupling coefficient and $\hat{\sigma}$ is the dc self-coupling coefficient defined as

$$\hat{\sigma} \equiv \delta + \frac{\sigma_{11} - \sigma_{22}}{2} - \frac{1}{2} \frac{d\phi}{dz}. \quad (2.6)$$

Here the detuning, which is assumed to be constant along z , is

$$\delta \equiv \frac{1}{2}(\beta^{co} - \beta^{cl}) - \frac{\pi}{\Lambda} = \pi \Delta n_{co} \left(\frac{1}{\lambda} - \frac{1}{\lambda_D} \right). \quad (2.7)$$

Here β^{co} and β^{cl} are the propagation constants related to the core and cladding modes, $\lambda_D \equiv \Delta n_{co} \Lambda$ is the design wavelength for an infinitesimally weak grating, Δn_{co} is the difference of the core and cladding effective indices, and Λ is the period of the long-period fiber grating. When appropriate initial conditions $A^{co}(0) = 1$ and $A^{cl}(0) = 0$ are specified, closed-form solutions can be found. The core mode and the cladding mode transmission coefficients for uniform long-period fiber gratings can be shown to be

$$T_{co} = \left| \frac{A^{co}(L)}{A^{co}(0)} \right|^2 = \cos^2(\sqrt{\kappa^2 + \hat{\sigma}^2} z) + \frac{1}{1 + \frac{\kappa^2}{\hat{\sigma}^2}} \sin^2(\sqrt{\kappa^2 + \hat{\sigma}^2} z) \quad (2.8)$$

$$T_{cl} = \left| \frac{A^{cl}(L)}{A^{co}(0)} \right|^2 = \frac{1}{1 + \frac{\hat{\sigma}^2}{\kappa^2}} \sin^2(\sqrt{\kappa^2 + \hat{\sigma}^2} z) \quad (2.9)$$

2.2 Transfer Matrix Method

Most fiber gratings designed for practical applications are not uniform gratings. For a long-period fiber grating with a non-uniform distribution of the coupling coefficient, no analytical solution can be found and only numerical solution can be calculated. One can use the piecewise-uniform approach to modeling non-uniform gratings, based on identifying 2×2 matrices for each uniform section of the grating, and then multiplying all of these together to obtain a single 2×2 matrix that describes the whole grating. We divide the long-period fiber grating with length L into m uniform sections and define A_i^{co} and A_i^{cl} to be the field amplitudes after traversing the section i . We start with $A_0^{co} = A^{co}(0) = 1$ and $A_0^{cl} = A^{cl}(0) = 0$, and calculate $A^{co}(L) = A_m^{co}$ and $A^{cl}(L) = A_m^{cl}$. The propagation through each uniform section i is described by a matrix F_i defined such that

$$\begin{bmatrix} A_i^{co} \\ A_i^{cl} \end{bmatrix} = F_i \begin{bmatrix} A_{i-1}^{co} \\ A_{i-1}^{cl} \end{bmatrix}. \quad (2.10)$$

$$F_i = \begin{bmatrix} \cos(\gamma\Delta) + \frac{i\hat{\sigma} \sin(\gamma\Delta)}{\gamma} & \frac{i\kappa \sin(\gamma\Delta)}{\gamma} \\ \frac{i\kappa^* \sin(\gamma\Delta)}{\gamma} & \cos(\gamma\Delta) - \frac{i\hat{\sigma} \sin(\gamma\Delta)}{\gamma} \end{bmatrix} \quad (2.11)$$

where Δ is the length of the i th uniform section for equal length $\Delta = \frac{L}{m}$, the coupling

coefficients $\hat{\sigma}$ and κ are the local values in the i th section, and $\gamma = \sqrt{\kappa^2 + \hat{\sigma}^2}$.

Once all of the matrices for the individual sections are known, we find the output amplitudes from

$$\begin{bmatrix} A^{co}(L) \\ A^{co}(L) \end{bmatrix} = F \begin{bmatrix} 1 \\ 0 \end{bmatrix} \quad (2.12)$$

where $F = \begin{bmatrix} F_{11} & F_{12} \\ F_{21} & F_{22} \end{bmatrix} = F_m \cdot F_{m-1} \cdot \dots \cdot F_1$

The transmission coefficients for the core and cladding modes are defined as

$$t_{co}(\delta) \equiv \frac{A^{co}(L, \delta)}{A^{co}(0, \delta)} = F_{11} \quad (2.13)$$

and

$$t_{cl}(\delta) \equiv \frac{A^{cl}(L, \delta)}{A^{co}(0, \delta)} = F_{21} \quad (2.14)$$

The power transmission coefficients for the core and cladding modes are then expressed

as

$$T_{co}(\delta) = |t_{co}(\delta)|^2 = |F_{11}|^2 \quad (2.15)$$

and

$$T_{cl}(\delta) = |t_{cl}(\delta)|^2 = |F_{21}|^2 \quad (2.16)$$



2.3 Evolutionary Programming Algorithm

2.3.1 Long-Period Fiber Gratings Synthesis Using Evolutionary

Programming [17]

1. Definition of the error function and the fitness function

We divide the spectral coordinate into n discrete wavelengths and randomly choose

N particular coupling coefficient distribution functions $\kappa_1(z), \kappa_2(z), \dots, \kappa_N(z)$, which are

complex vectors with m components. The error function and fitness function for the $\kappa_i(z)$

are defined as

$$\mathcal{E}(\kappa_i) \equiv \sum_{\ell=1}^n |T_{\text{target},\ell} - T_{i,\ell}| \quad (2.17)$$

and

$$F(\kappa_i) \equiv \frac{1}{\mathcal{E}(\kappa_i)} \quad (2.18)$$

$i = 1, 2, \dots, N$

where $T_{\text{target},\ell}$ is the target transmission coefficient at the ℓ th wavelength component and $T_{i,\ell}$ is the power transmission coefficient produced by $\kappa_i(z)$ at the ℓ th wavelength component.



2. Selection

The originally chosen set of N individuals $\kappa_i(z), i = 1, 2, \dots, N$ is the parent set. The $\kappa_i(z)$ with a higher fitness value will have a higher probability to be chosen. The probability of each $\kappa_i(z)$ being selected is

$$P(\kappa_i(z)) = \frac{F(\kappa_i)}{\sum_{j=1}^N F(\kappa_j)}, i = 1, 2, \dots, N \quad (2.19)$$

After applying the selection process to the parent set, it generates a set of new individuals from the parent set which we call it a “healthier” set because the average fitness value of the new set is usually larger than the parent set.

3. Mutation

For a given coupling coefficient profile $\kappa_i(z)$, we randomly choose one of is

components $\kappa_{i,j}(z) = |\kappa_{i,j}| e^{i\phi_{i,j}}$ and change it into

$$\widehat{\kappa}_{i,j}(z) = |\kappa_{i,j} + \delta\kappa_{i,j}| e^{i(\phi_{i,j} + \delta\phi_{i,j})}, i = 1, 2, \dots, N \quad (2.20)$$

where $\delta\kappa_{i,j}$ and $\delta\phi_{i,j}$ are the magnitude and phase mutation functions, respectively, and are determined by the following expressions

$$\delta\kappa_{i,j} = r_{M,i} \times W_i \quad (2.21)$$

$$\delta\phi_{i,j} = r_{s,i} \times W_i \quad (2.22)$$

where $r_{M,i}$ and $r_{s,i}$ are two random variables between -1 and 1 and W_i is a weighting factor calculated according to

$$F^q(\kappa_i) \cdot W_i = C \quad (2.23)$$

where C and q are adjustable numbers called the mutation parameters.

To summarize, we describe the process of our evolutionary programming algorithm by the flow chart show in Fig. 2.1 and explain how it works as follows.

1. Divide the spectral coordinate into n discrete wavelengths to be the target.
2. Generate a set of N coupling coefficient profiles by selecting the value of their components randomly within a feasible range. This is the parent set with N individuals $\kappa_i(z), i = 1, 2, \dots, N$.
3. Calculate the transmission spectrum for each coupling coefficient profile in the parent set by using the coupled-mode equation and the transfer matrix method of long-period fiber gratings previously described in chapter 2.

4. Find the error and the fitness value for each $\kappa_i(z), i = 1, 2, \dots, N$ in the parent set.
5. Check if the target performance is reached for any individual in the parent set. If not, apply the selection process to the parent set to generate a set of “healthier” individuals.
6. Apply the mutation process to create a new set of N individuals from the “healthier” set in step 5. Go to step 3 and use the new set as the parent set.

2.3.2 Simulation of Flat-Band Long-Period Fiber Gratings

The target spectra of a flat-band long-period fiber grating can be described by [22]

$$|S(\delta)| = \sqrt{0.9} \exp\left(-\left(\frac{\delta}{\delta_{FWHM}}\right)^{10}\right) \quad (2.24)$$

$$|R(\delta)| = \left(1 - 0.9 \exp\left(-\left(\frac{\delta}{\delta_{FWHM}}\right)^{20}\right)\right)^{1/2} \quad (2.25)$$

where $\delta = \pi \Delta n_{eff} \left(\frac{1}{\lambda} - \frac{1}{\lambda_D}\right)$ is the detuning parameter, δ_{FWHM} is the

full-width-half-maximum bandwidth. In our simulation, we set the grating length $L=97.5$

mm , the number of section $m=15$, the section width $\Delta z=6.5$ mm , the number of spectral

points $n=161$, the grating period $\Lambda=0.26$ mm and the resonance wavelength $\lambda_D=1550$ nm .

The core and cladding mode indices are assumed to be

$$n_{co} = 1.450250813 - 0.0108 * (\lambda - 1.55) \quad (2.26)$$

$$n_{cl}(\lambda) = \left[1 + \frac{0.6961663 \cdot \lambda^2}{\lambda^2 - 0.0684043^2} + \frac{0.4079426 \cdot \lambda^2}{\lambda^2 - 0.1162414^2} + \frac{0.897479 \cdot \lambda^2}{\lambda^2 - 9.896161^2}\right]^{\frac{1}{2}} \quad (2.27)$$

Fig. 2.2 shows the target spectrum and the calculated spectrum form our design. Fig. 2.3

and 2.4 show the designed amplitude and phase profiles of the coupling coefficient across the grating, respectively.



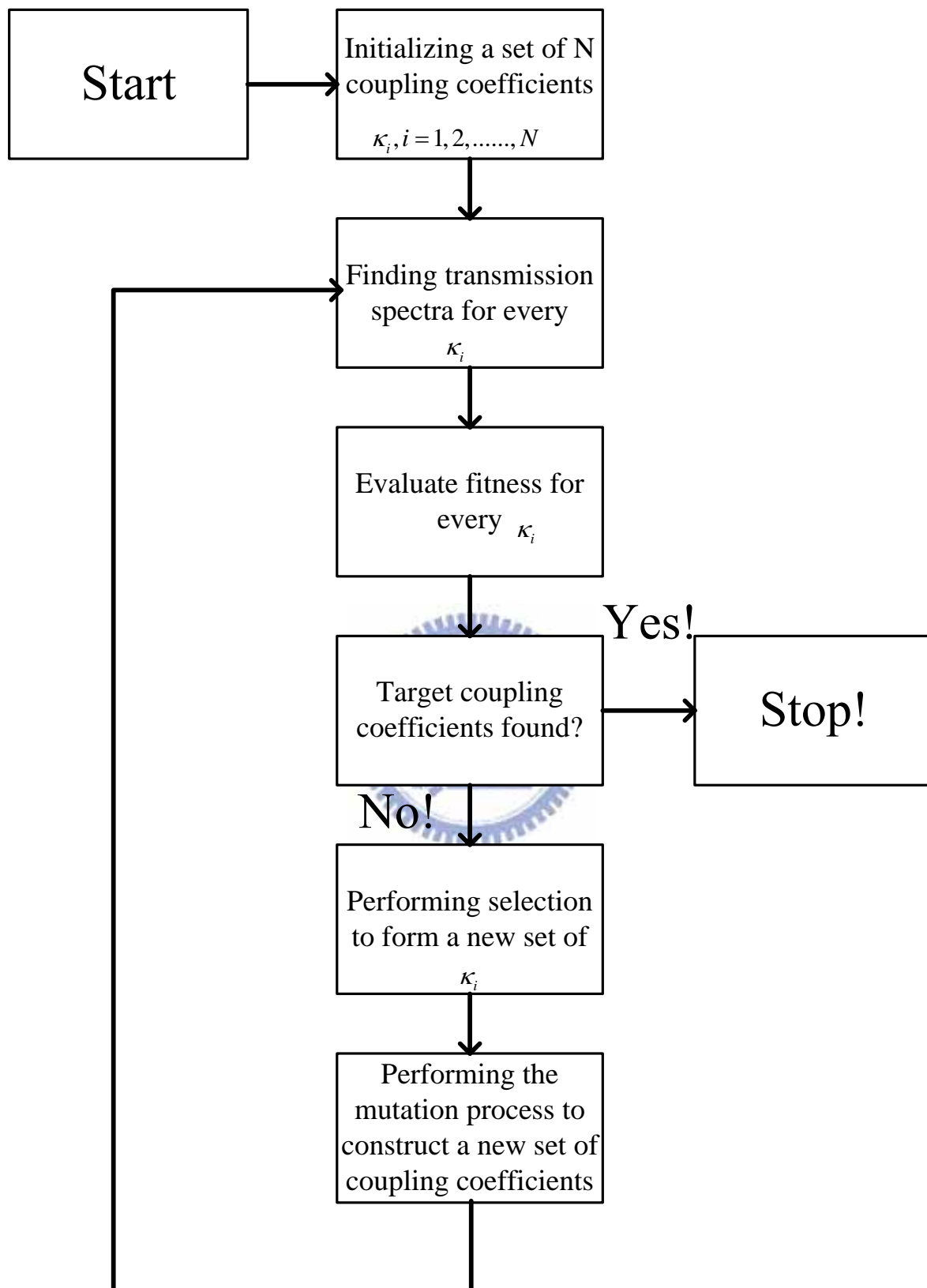


Fig. 2.1 Flow chart of the proposed EP algorithm for LPG design

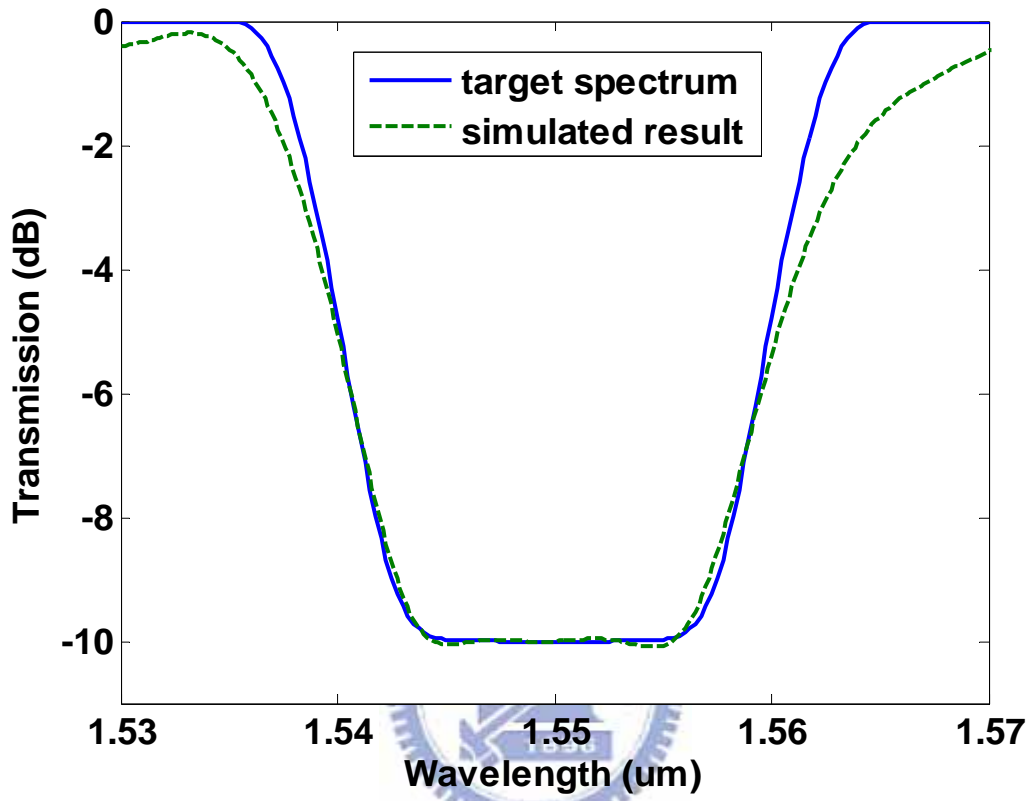


Fig. 2.2 Target and designed transmission spectra of the flat-band LPG.

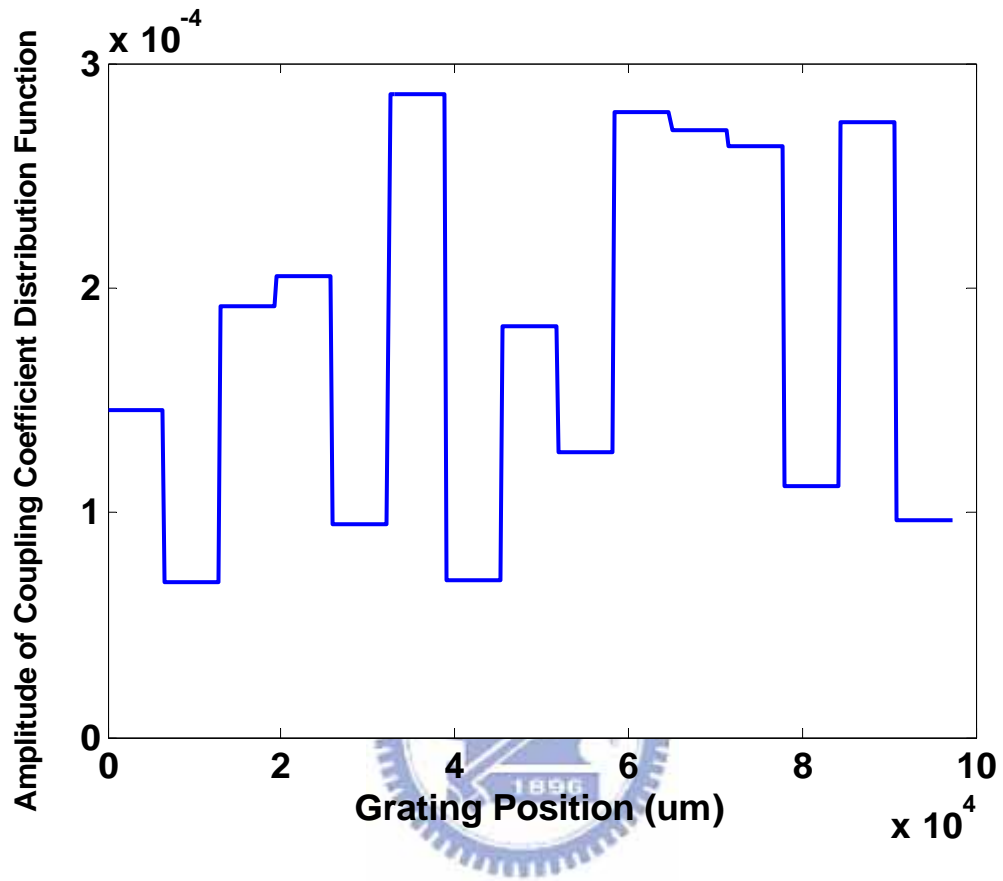


Fig. 2.3 Designed amplitude of the coupling coefficient distribution function for the flat-band LPG.

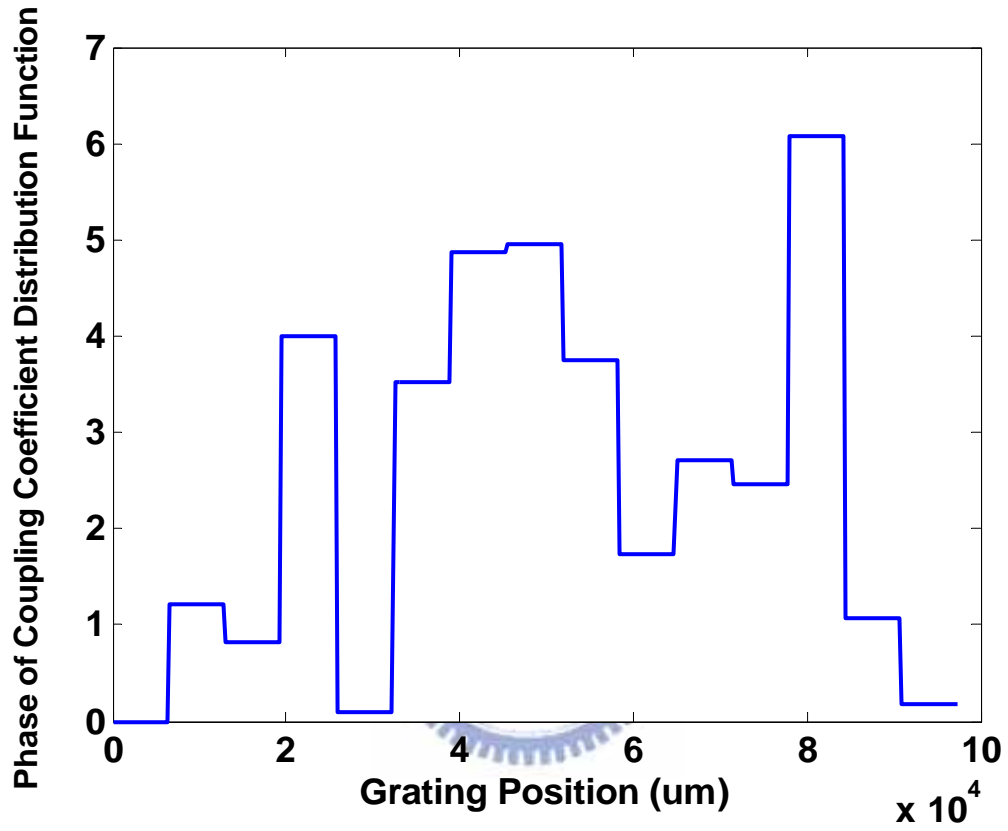


Fig. 2.4 Designed phase of the coupling coefficient distribution function for the flat-band LPG.

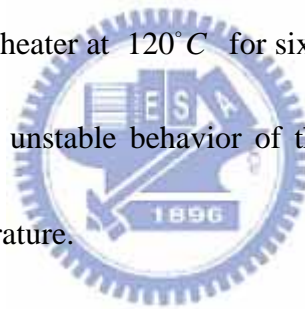
Chapter 3. Experimental Setup and Results

3.1 Experimental Setup

The fiber we used is the PS1250-1500 photosensitive fiber from Fibercore Company. In order to achieve the special coupling coefficient profile, we fabricate the phase-shifted long period fiber gratings by the point-by-point UV writing method. Fig. 3.1 shows the experimental setup. A frequency-doubled argon-ion laser launches a CW 244 nm single-polarization UV beam which passes through three cylindrical lens 1, 2 and 3 and then is focused on a fiber with its e^{-1} beam waist $<100 \mu m$. The UV beam-shape is an elliptical shape and the major axis is along the x-direction before the laser beam passes through the cylindrical lens 1 and cylindrical lens 2. The cylindrical lens 1 and 2 are used to expand the UV beam and the cylindrical lens 3 is used to focus the UV beam in the x-direction to the fiber. After focusing, the UV beam becomes an elliptical beam with the major axis along the y-direction. The UV power is confined in the region of the writing point, so that it can induce the change of the refractive index in core as much as 4.5×10^{-4} in ten seconds without hydrogen-loading the fiber. The induced refractive index can be adjusted by controlling the exposure time. With hydrogen loading, the order of induced refractive index change can be further improved, and the UV induced index change will be increased while we increase the hydrogen loading duration up to the saturation time. However, it is not easy to control the

hydrogen loading concentration of the fibers in practice. The hydrogen will begin to escape from the fibers when we put the loaded fibers in the air. To avoid this uncertainty, we used non-hydrogen loading fibers in our experiment.

A shutter is used in the halfway of the beam path. The induced refractive index change in the core of the fiber is related to the UV exposure time, which can be modulated by the shutter. The fiber is put on a translation stage which consists of a linear motor stage and a piezoelectric translator (PZT) stage with sub-nm position resolution. The position of the exposed points on the fiber can be accurately controlled by such a translation stage. After the UV exposure, the fiber is put on a heater at 120°C for six hours for annealing. The annealing process is to avoid the thermally unstable behavior of the exposed fiber grating over long periods of time at the room temperature.



3.2 Calibration of the Parameters

1. Choose the cladding mode LP08

By using the super-luminescent diode (SLD) broadband light source (from 1250 nm to 1650 nm) and the optical spectrum analyzer (OSA), we can identify different coupled cladding modes by changing different grating periods, and then determine the suitable mode and grating period for us to use. Fig. 3.2 to 3.5 shows the transmission spectra at different grating periods. First, we use the spectrum at the grating period of $450\ \mu\text{m}$ to identify the

first coupled cladding mode LP02. We then reduced the grating period to $430\ \mu\text{m}$, $420\ \mu\text{m}$, $350\ \mu\text{m}$ and $210\ \mu\text{m}$, respectively. From these spectra, we can recognize LP03 to LP08 modes and find that the change rates of the dips in the transmission spectra increase from LP02 to LP08 modes. At the grating period of $210\ \mu\text{m}$, there is only the LP08 mode observed. By the consideration of the laser beam size focused on fiber (less than $100\ \mu\text{m}$, e^{-1}), the duty cycle we desired (about 50%) and the change rates of the spectral dips, we choose the LP08 mode as the coupled cladding mode. We then choose $260\ \mu\text{m}$ as the grating period, under which the center wavelength of the LP08 mode dip is in the region of C band, which is between $1520\ \text{nm}$ and $1570\ \text{nm}$.

2. Use uniform long-period fiber gratings to calibrate n_{co} and Δn

After the identification of the coupling cladding mode and the grating period, an ASE broadband light source (from $1520\ \text{nm}$ to $1620\ \text{nm}$) and an optical spectrum analyzer (OSA) are used to measure the transmission spectra of the LPGs. We use uniform long-period fiber gratings as the reference to calibrate the core refractive index change versus wavelength and the modulated refractive index change versus time. We assume that the relation of the core refractive index change versus wavelength is linear between $1520\ \text{nm}$ and $1620\ \text{nm}$ and the dispersion relation of the cladding material is equal to that of pure silica. From the experimental results, the dispersion relation of core is $n_{co} = 1.450250813 - 0.0108 * (\lambda - 1.55)$.

The relation between the refractive index change and the exposure time is

$\Delta n = 1.8623 + 0.9631 * \ln(t)$, which was fitted by the Napierian logarithm. Fig. 3.6 shows the real core refractive index change versus wavelength. From it, we can get the slope $\frac{dn_{co}}{d\lambda} = 0.0108$ and $n_{co} = 1.450250813$ at 1550 nm . Fig. 3.7 shows the modulated refractive index change versus time, and it illustrates that the relation between the refractive index change and the exposure time is not linear. From the figure, the change of refractive index in core is about 4.5×10^{-4} with the exposure time of ten seconds. We thus limit the maximum induced refractive index to 4.5×10^{-4} in the simulation.

3.3 Simulation and Experimental Results

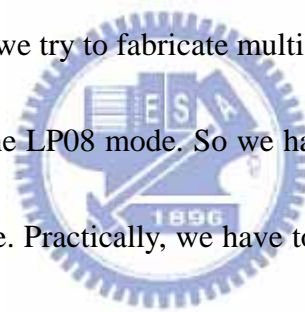
3.3.1 Uniform Long-Period Fiber Gratings

We use the parameters from the calibration to run the simulation. Figures 3.8 to 3.14 show the comparison between the simulation results and the experimental results at the exposure time of 1s, 2s, 3s, 4s, 6s, 8s and 10s. From these figures, we find that the bandwidth of the grating transmission spectra match well with simulation results, but their center wavelengths have slight difference. This difference may be mainly caused by the tight force we used to fix the fiber when exposing the grating or when measuring the fiber grating spectrum. The extra tension may slightly change the grating period of the fiber grating.

3.3.2 Simple Phase-Shifted Long-Period Fiber Gratings

The explored simple phase-shifted long-period fiber gratings in this section include single phase-shifted, double phase-shifted and multi-phase-shifted (less than ten shifted phases) long-period fiber gratings. Fig. 3.15 to 3.17 show the structures of these simple phase-shifted long-period fiber gratings. Our simulated and experimental spectral results are shown in Fig. 3.18 to 3.23. From these figures, we find that the dips in the grating transmission spectra do not well match the prediction depth for deep dips. This is because when it is closed to the zero transmission, the depth is more sensitive in the dB scale.

There is another reason why we try to fabricate multi-phase-shifted LPGs for verification. In simulation, we only consider the LP08 mode. So we have to avoid the spectra of the other modes to mix with the LP08 mode. Practically, we have to confirm that how many periods of a uniform section is enough to avoid the spectra of the other modes to mix with that of the LP08 mode. In Fig. 3.22, we can confirm that the LPG with 20 periods in a uniform section is safe. That means the LPGs with every uniform region containing more than 20 periods can be used in our simulation and fabrication.



3.3.3 Flat-Band Long-Period Fiber Gratings

After calibration, we used these parameters to design a flat-band LPG. We use the theory mentioned in chapter 2 and the MATLAB software to write a synthesis program for the

defined target. The designed result and its corresponding coupling coefficient distribution function of the flat-band LPG have been mentioned before (in 2.3.2 Simulation of Flat-Band Long-Period Fiber Gratings, Chapter 2.). Fig. 3.24 shows the comparison of the simulated and experimental results of the flat-band LPG. For the first sight, the experimental result seems to be quite different from the simulated result. The center wavelength of the experimental result slightly shifts to the longer wavelength. Moreover, the grating transmission spectrum is not a flat band but more like a dip, and the bandwidth is narrower than the simulated one. We believe this is mainly caused by the difference between the fabricated and simulated coupling coefficient distribution functions, which are complicatedly dependent on the induced refractive index change, the fringe visibility of the index change, the core refractive index at designed wavelength, the mode profiles, etc. To explore more deeply, Fig. 3.25(a) and Fig. 3.25(b) show the simulated spectra with different ratios of the coupling coefficient distribution functions when compared to the original one. From these figures, we find that when the ratio of the coupling coefficient distribution function changes from 0.85 to 1.15, the center wavelength and the dip of the spectra also move from shorter wavelengths to longer wavelengths. Moreover, the simulated spectra are getting deeper from shorter wavelengths to longer wavelengths. Fig. 3.26(a) and Fig. 3.26(b) show the simulated spectra at different fringe visibilities of the index change when compared to the original one. They illustrates that when the fringe visibility of the index change is changed from $2*0.75$ to $2*0.95$, the center



wavelength and the dip of the spectra have the similar behavior compared to Fig. 3.25(a) and Fig 3.25(b), but the depth of the band is not changed. In the spectrum with $v=2*0.95$, we find that the shape is quite similar to our experimental result, except that its center wavelength moves to the shorter wavelengths. Based on these simulated results, we believe the main error in the fabrication should be caused by the difference in the fringe visibility of the index change between the fabricated coupling coefficient distribution function and the simulated one.



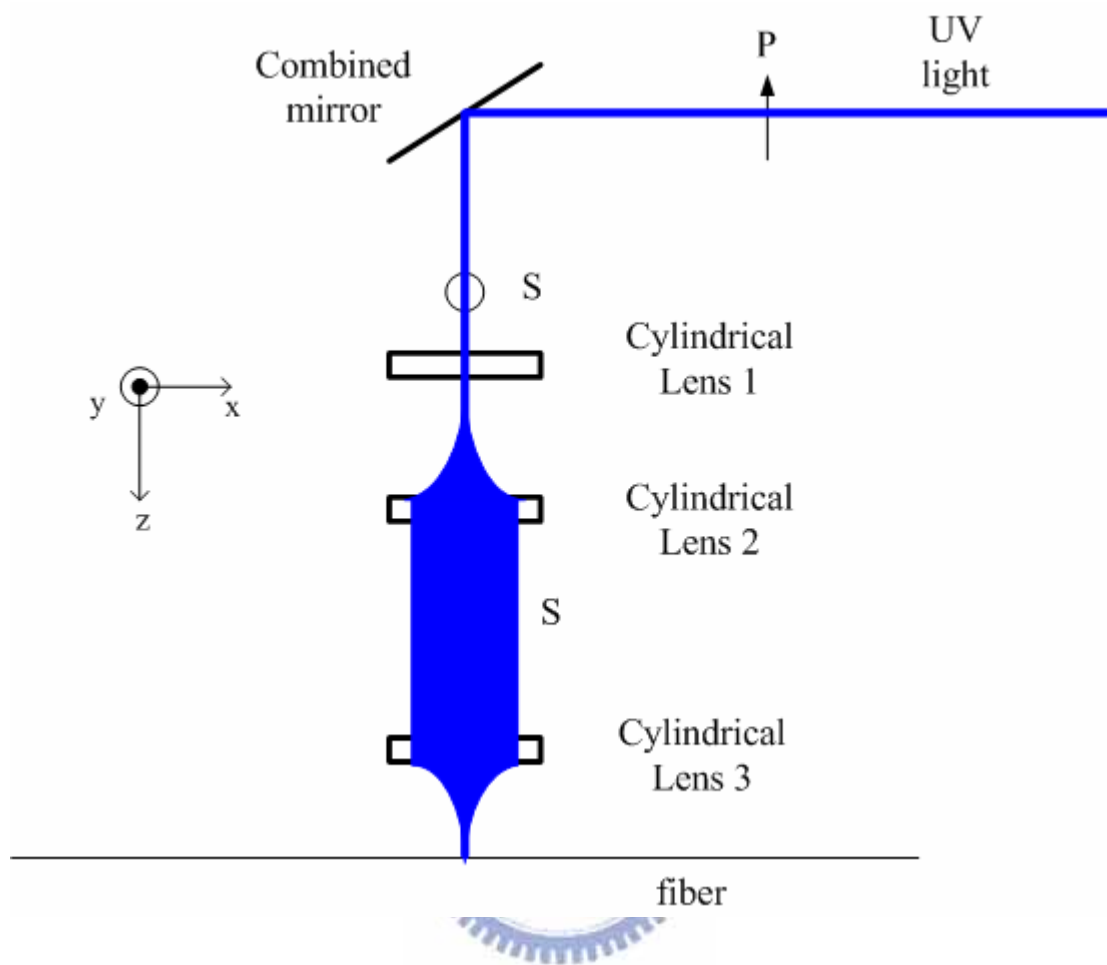


Fig. 3.1 Experimental setup of sequential point writing

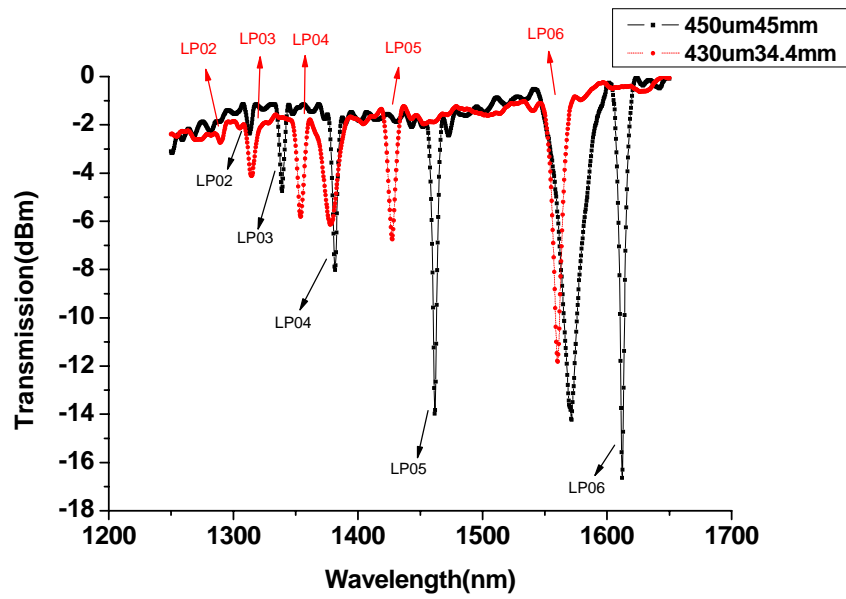


Fig. 3.2 Transmission spectra for LPGs with different grating periods ($450 \mu m$ and $430 \mu m$)

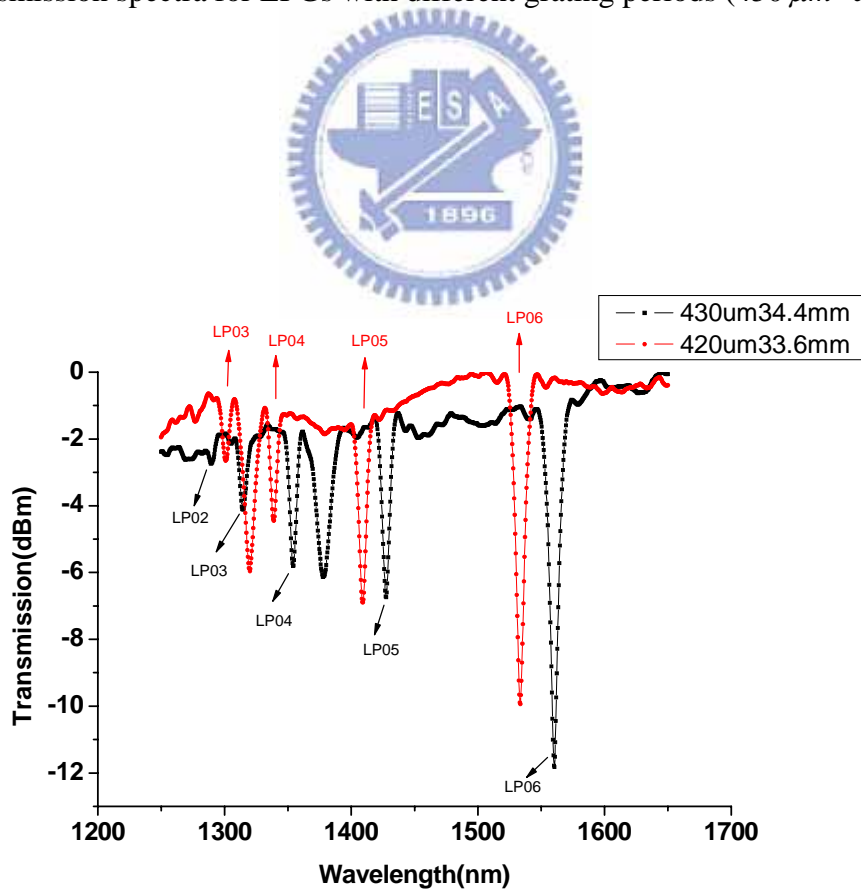


Fig. 3.3 Transmission spectra for LPGs with different grating periods ($430 \mu m$ and $420 \mu m$)

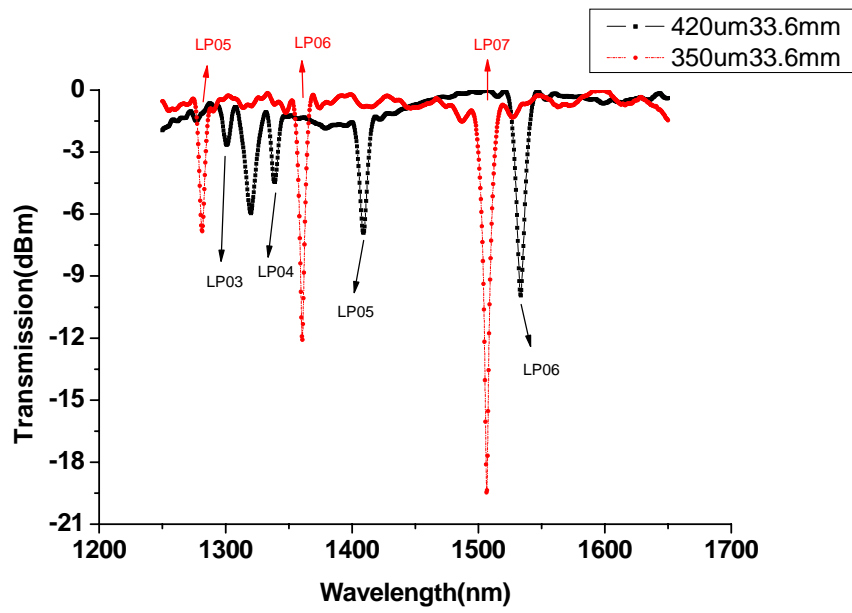


Fig. 3.4 Transmission spectra for LPGs with different grating periods ($420 \mu m$ and $350 \mu m$)

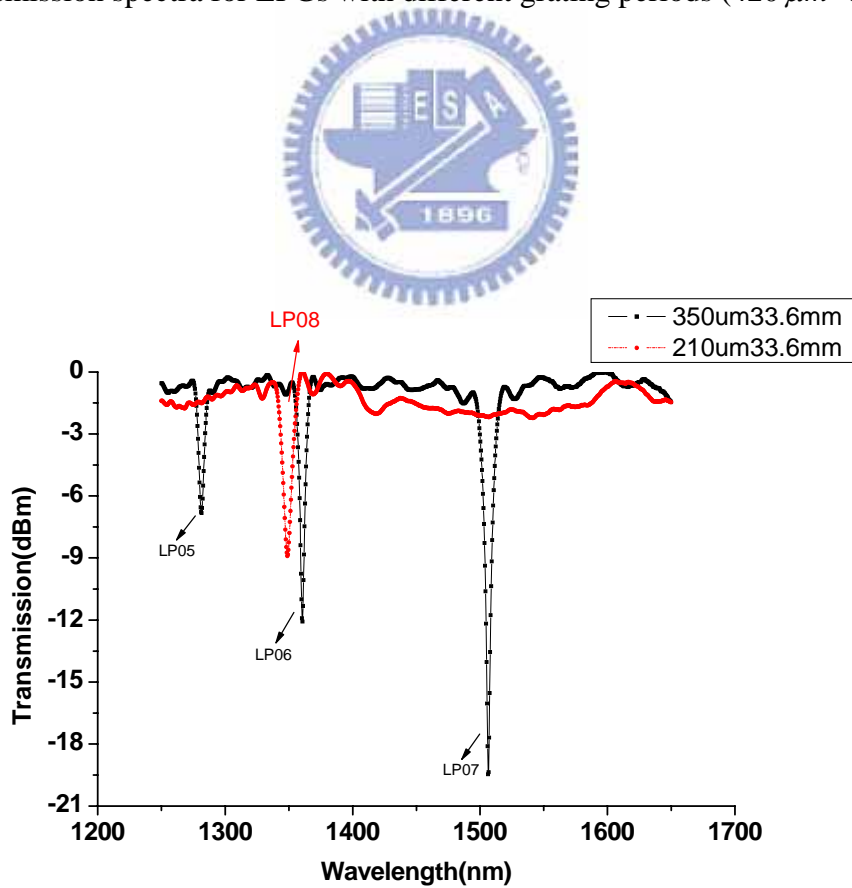


Fig. 3.5 Transmission spectra for LPGs with different grating periods ($350 \mu m$ and $210 \mu m$)

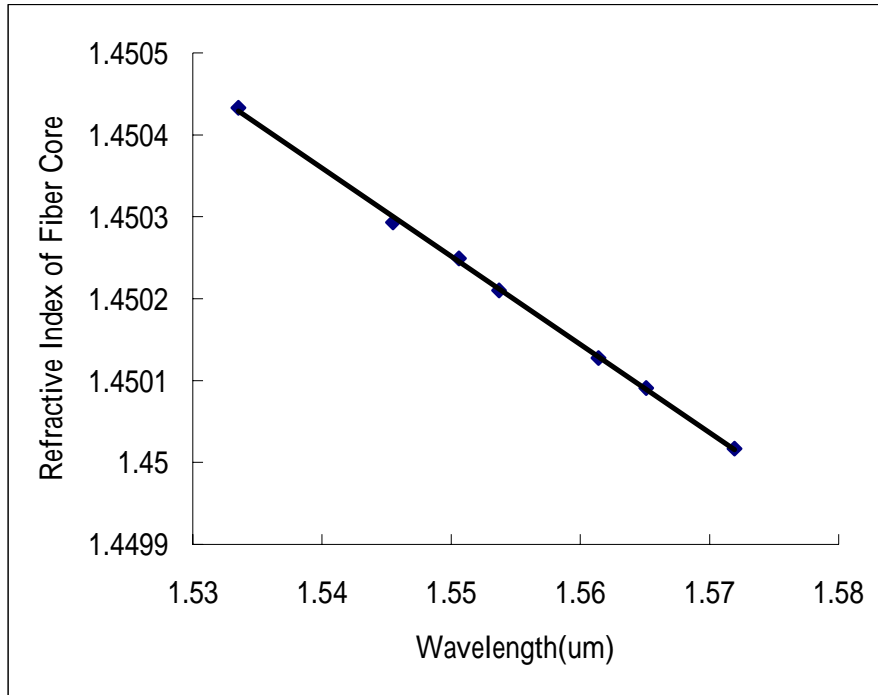


Fig. 3.6 The core refractive index change versus wavelength

$$n_{co} = 1.450250813 - 0.0108 * (\lambda - 1.55)$$

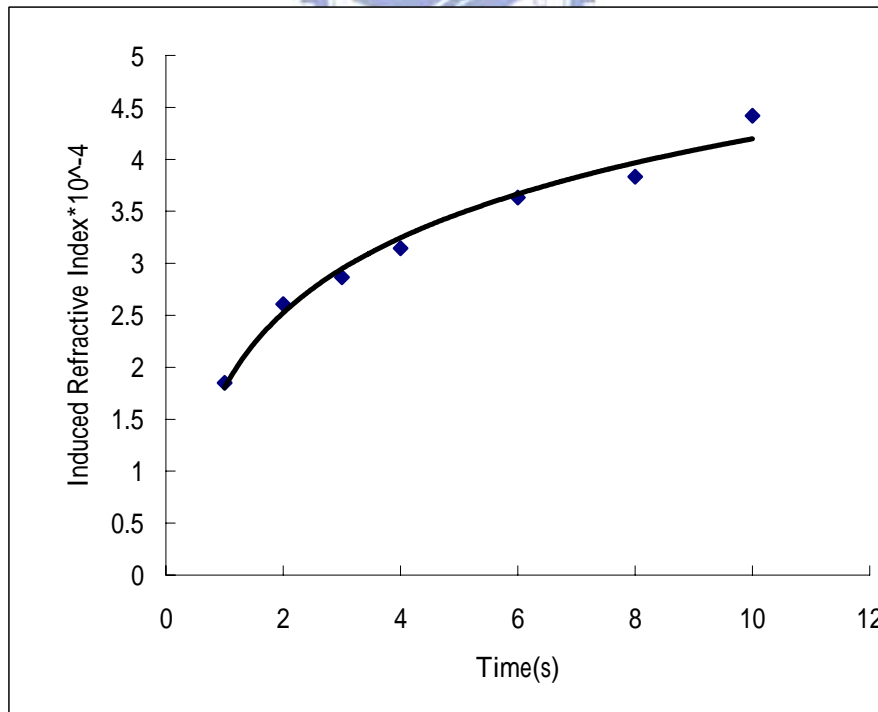


Fig. 3.7 The modulate refractive index change versus time

$$\Delta n = 1.8623 + 0.9631 * \ln(t)$$

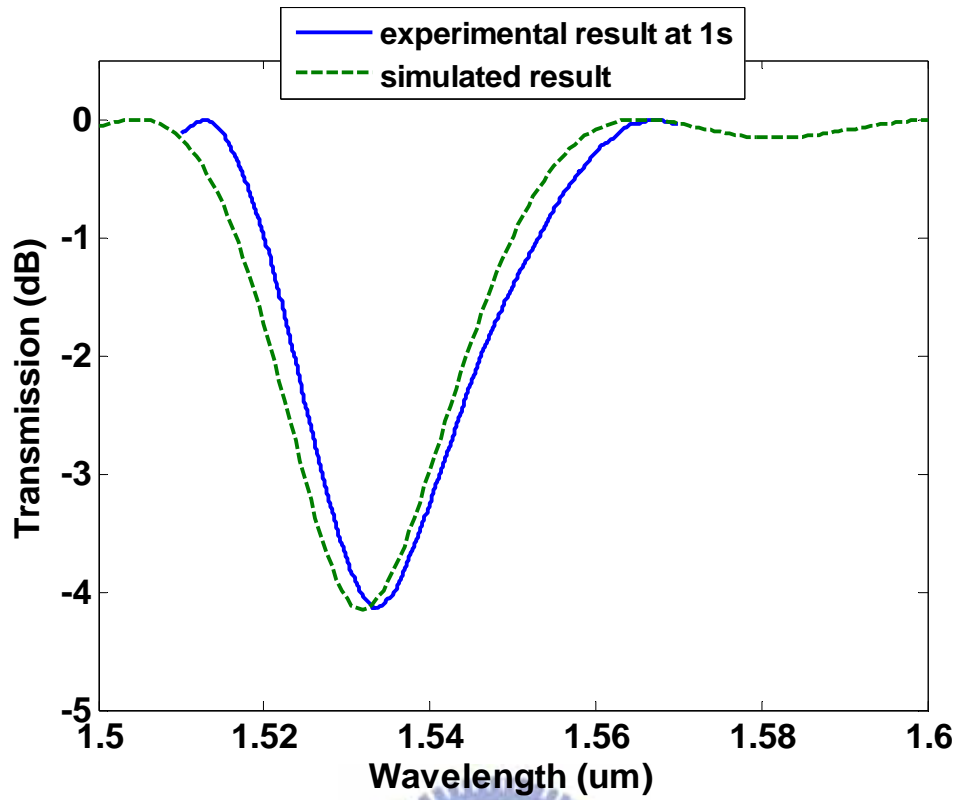


Fig. 3.8 Transmission spectra for uniform LPG (exposure time = 1s)

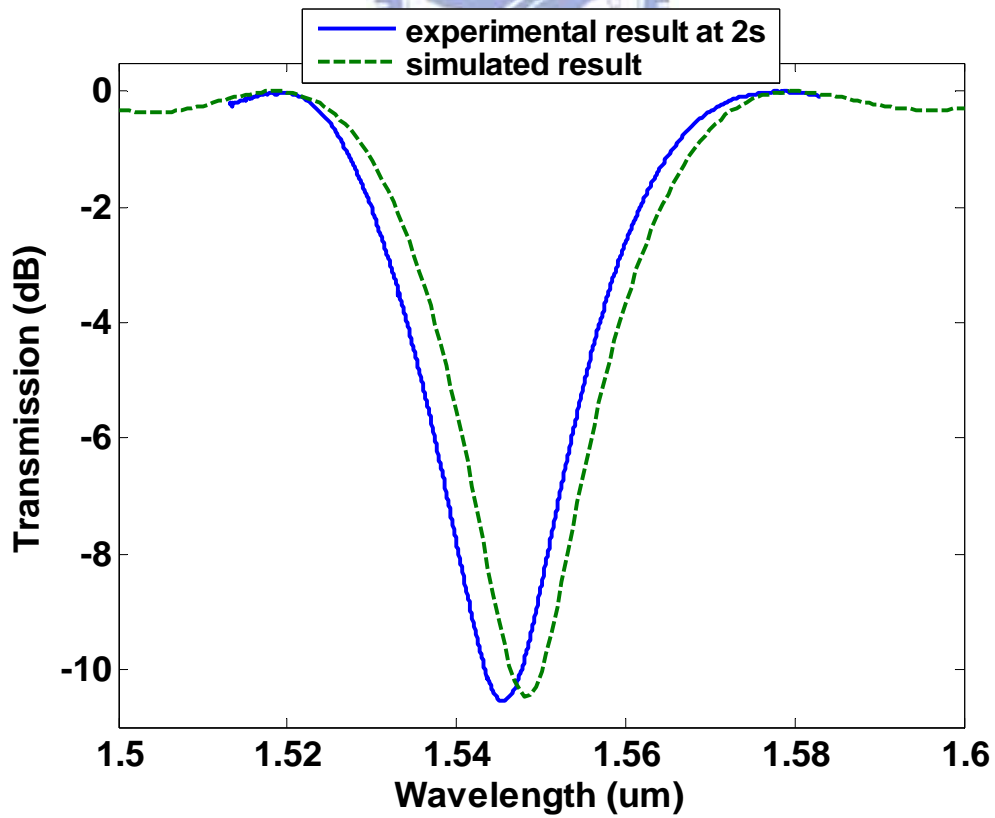


Fig. 3.9 Transmission spectra for uniform LPG (exposure time = 2s)

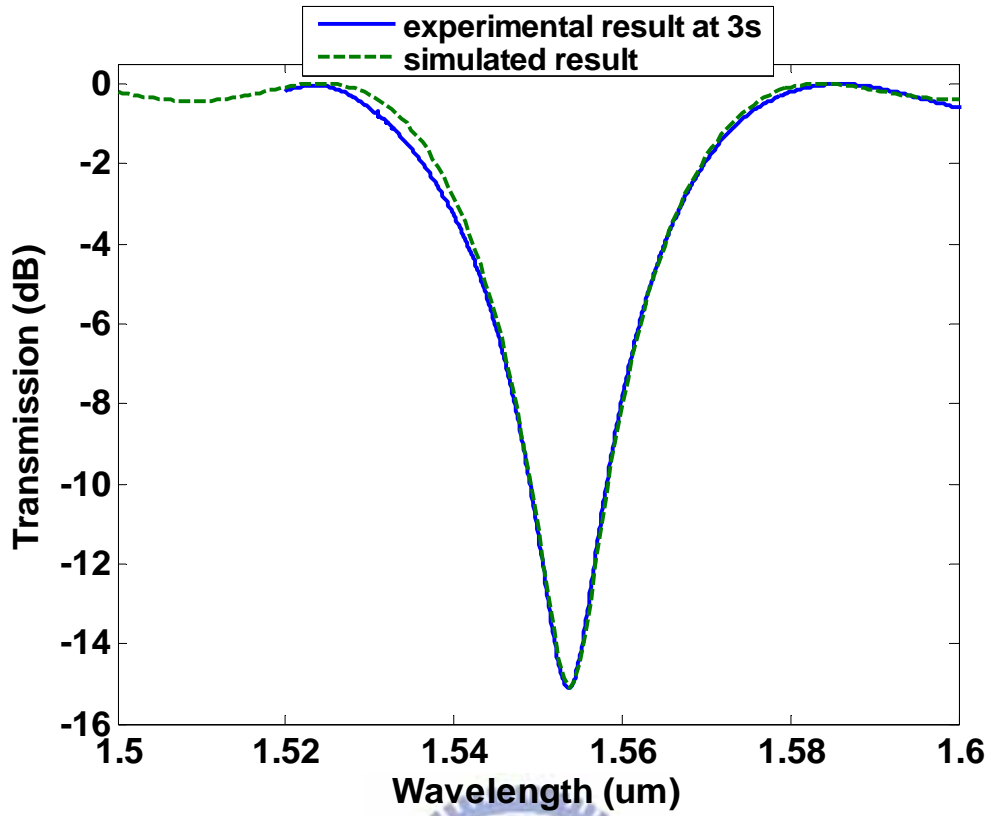


Fig. 3.10 Transmission spectra for uniform LPG (exposure time = 3s)

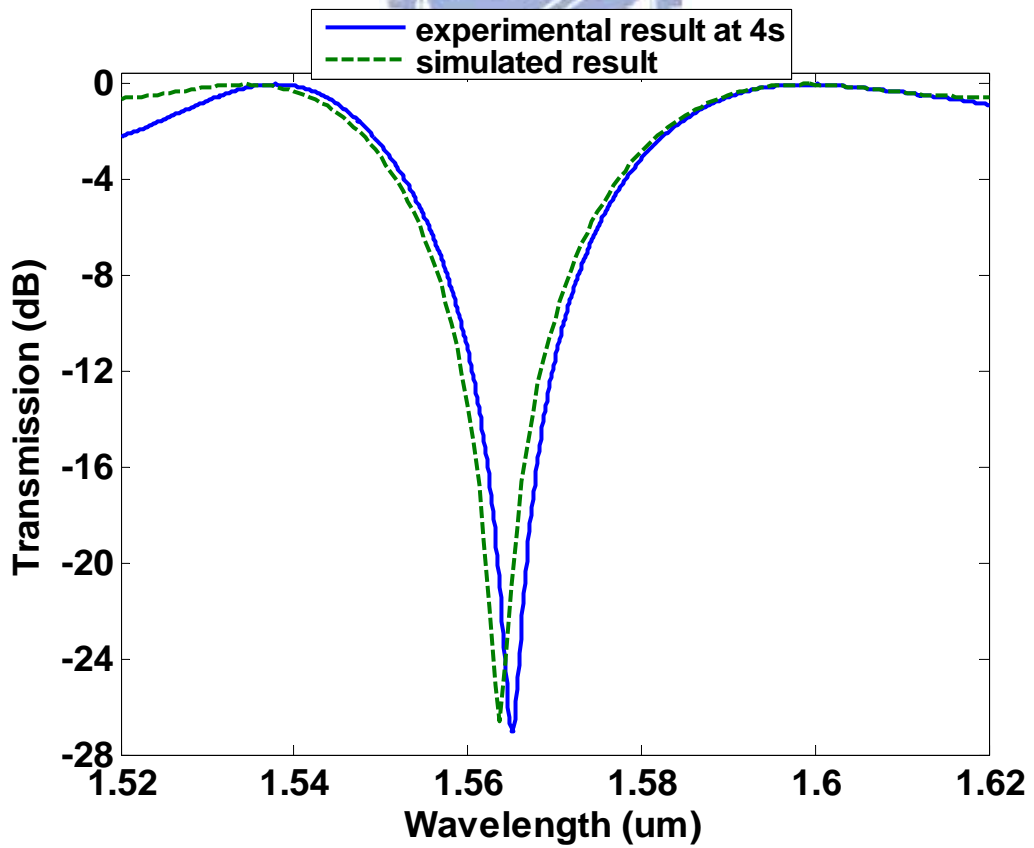


Fig. 3.11 Transmission spectra for uniform LPG (exposure time = 4s)

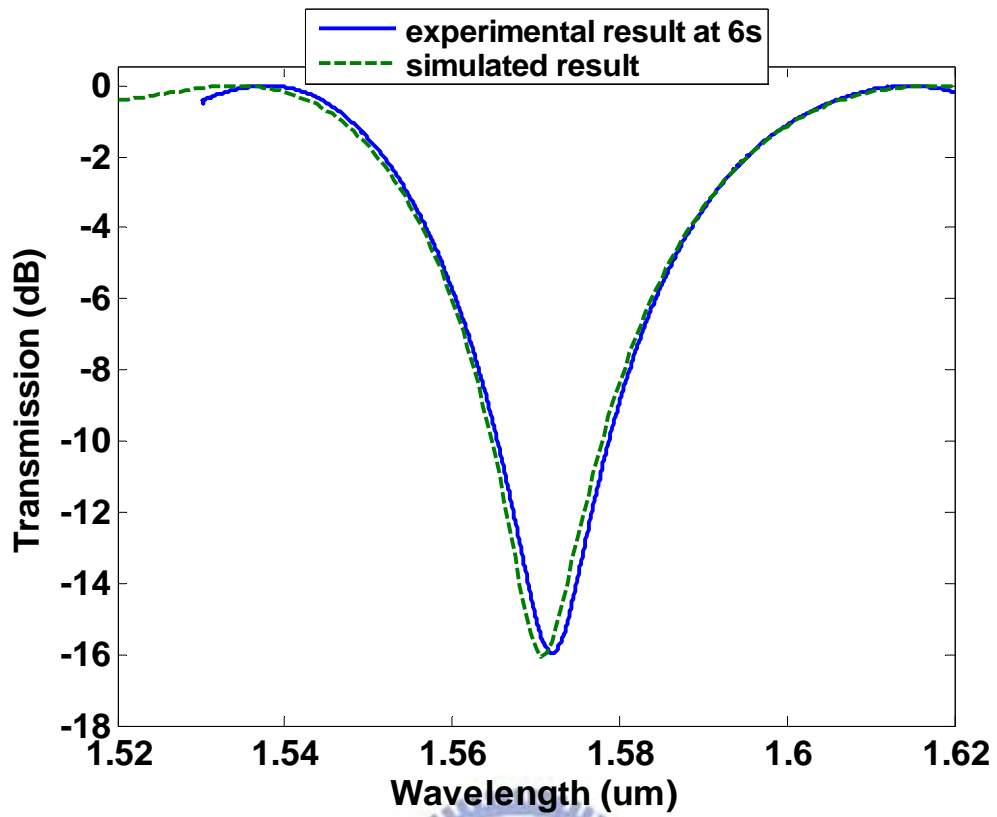


Fig. 3.12 Transmission spectra for uniform LPG (exposure time = 6s)

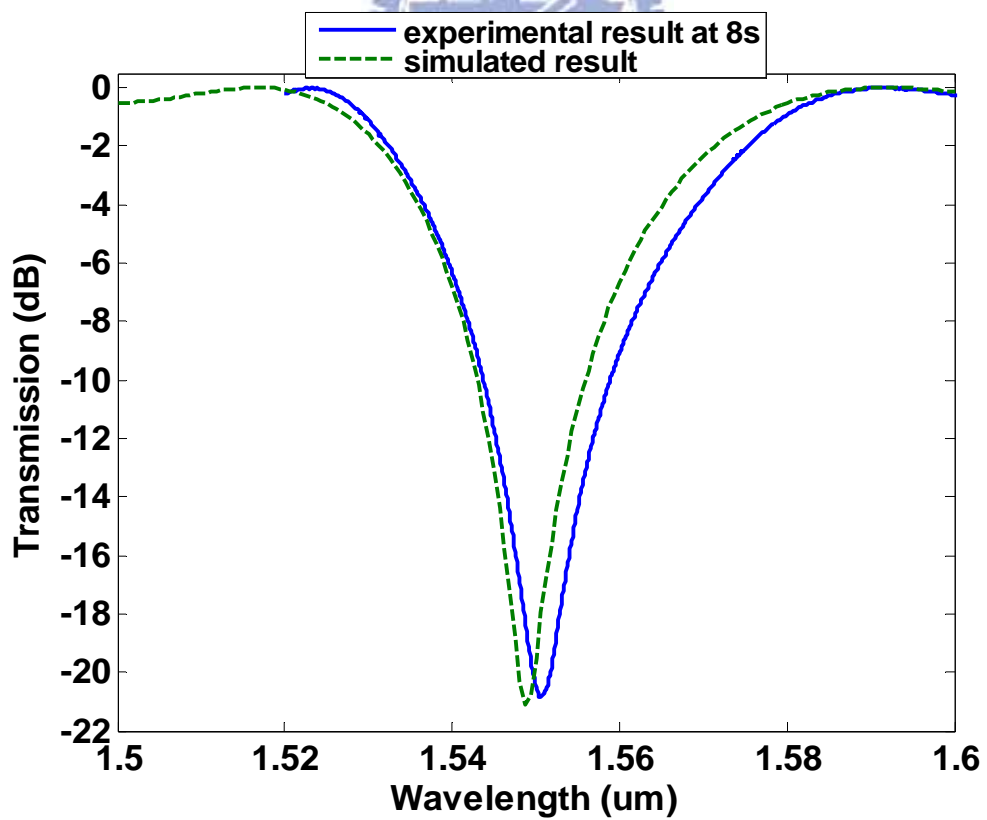


Fig. 3.13 Transmission spectra for uniform LPG (exposure time = 8s)

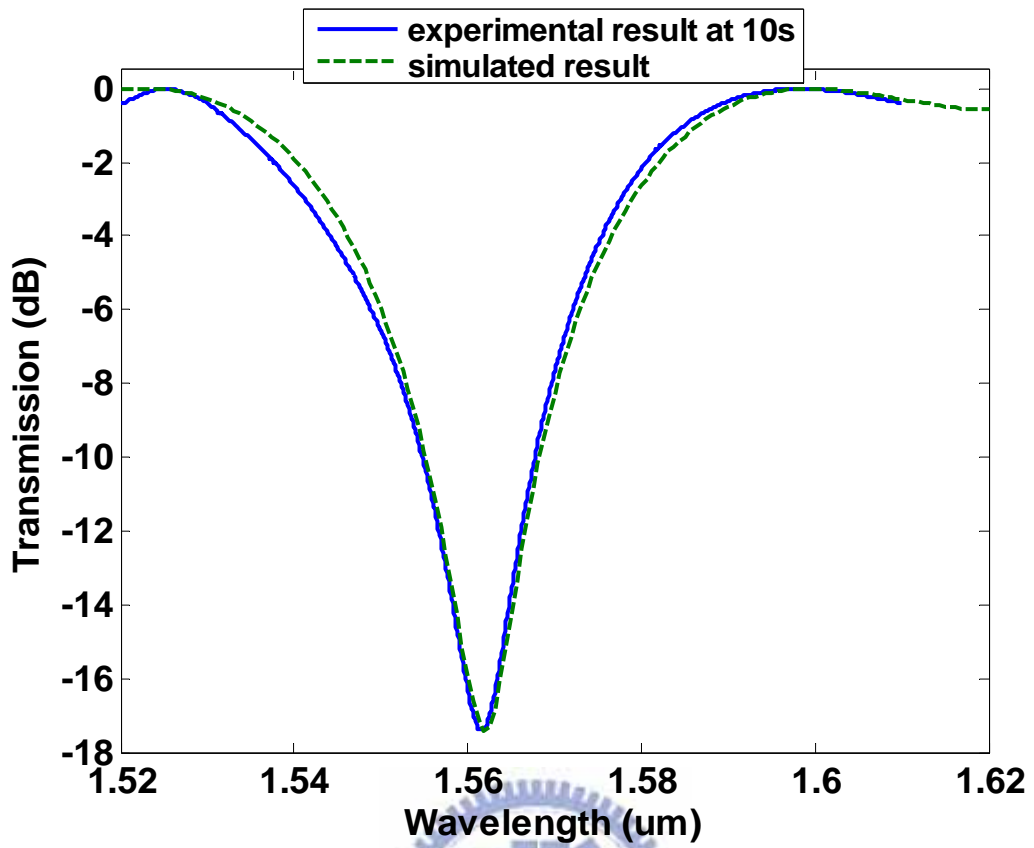


Fig. 3.14 Transmission spectra for uniform LPG (exposure time = 10s)



Single phase-shifted

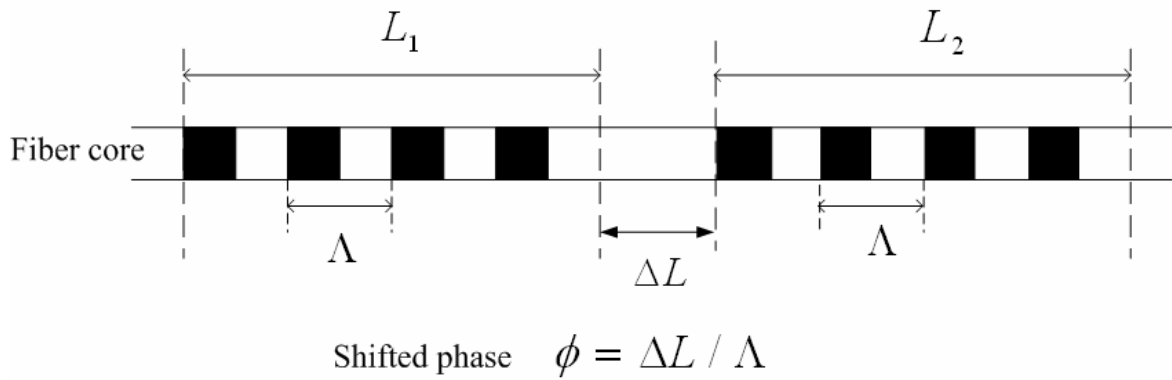


Fig. 3.15 Single phase-shifted LPG

Double phase-shifted

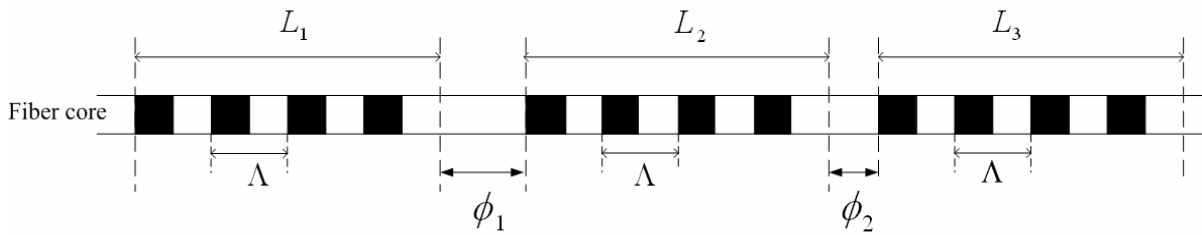


Fig. 3.16 Double phase-shifted LPG

Multi-phase-shifted

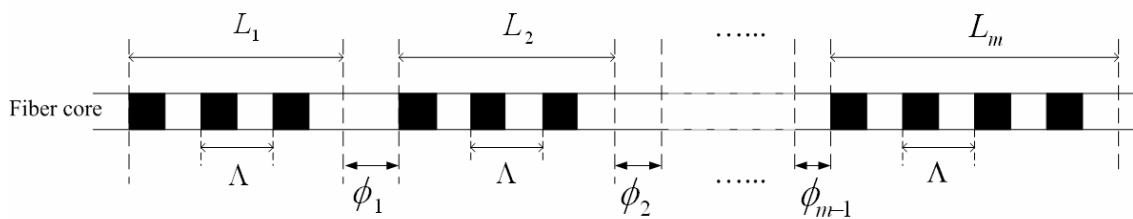


Fig. 3.17 Multi-phase-shifted LPG

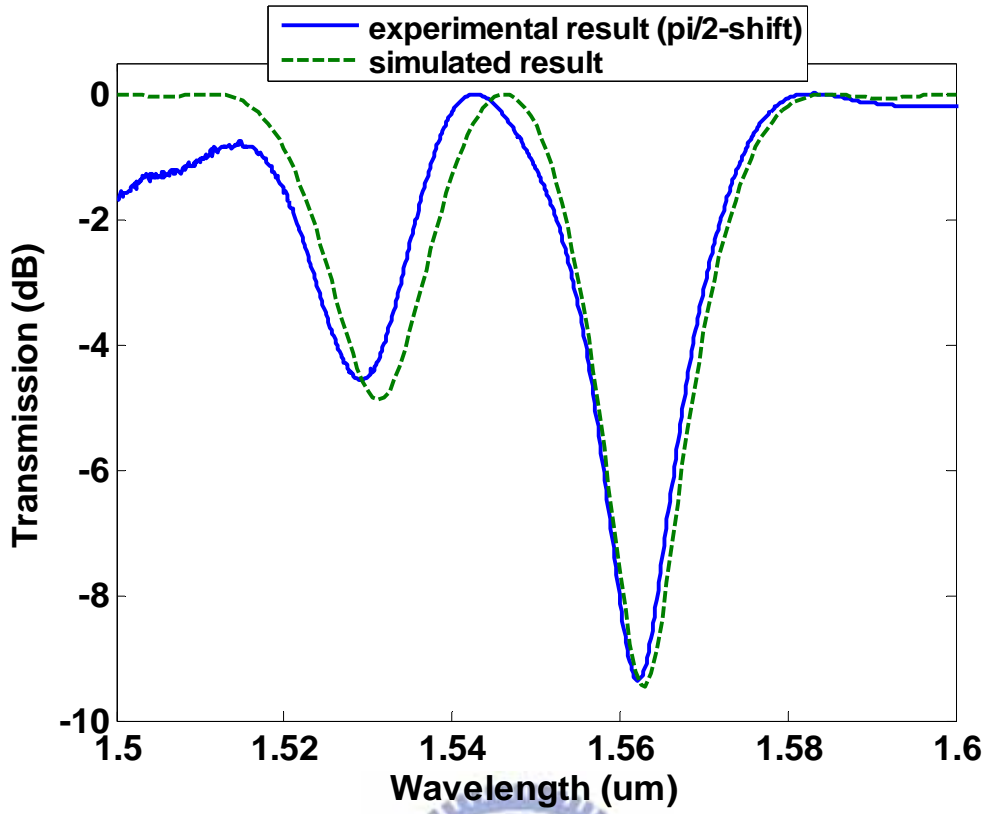


Fig. 3.18 Transmission spectra for single phase-shifted LPG ($L_1 = L_2 = 19.5\text{mm}$, $\phi = \pi / 2$)

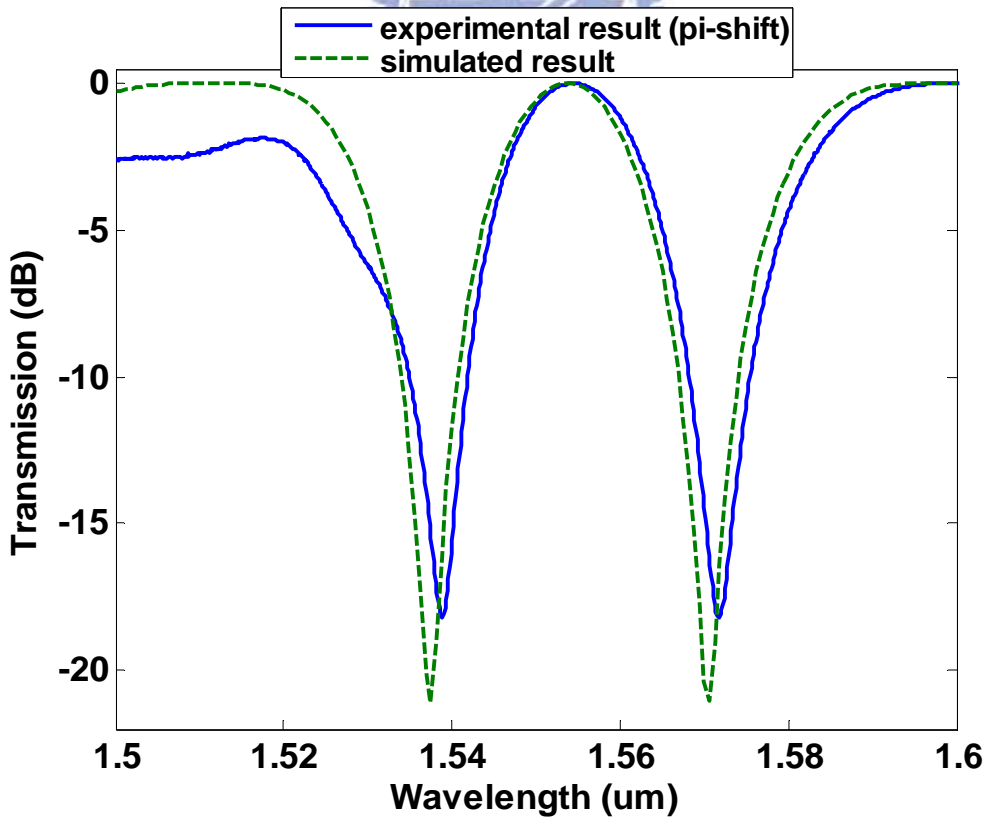


Fig. 3.19 Transmission spectra for single phase-shifted LPG ($L_1 = L_2 = 19.5\text{mm}$, $\phi = \pi$)

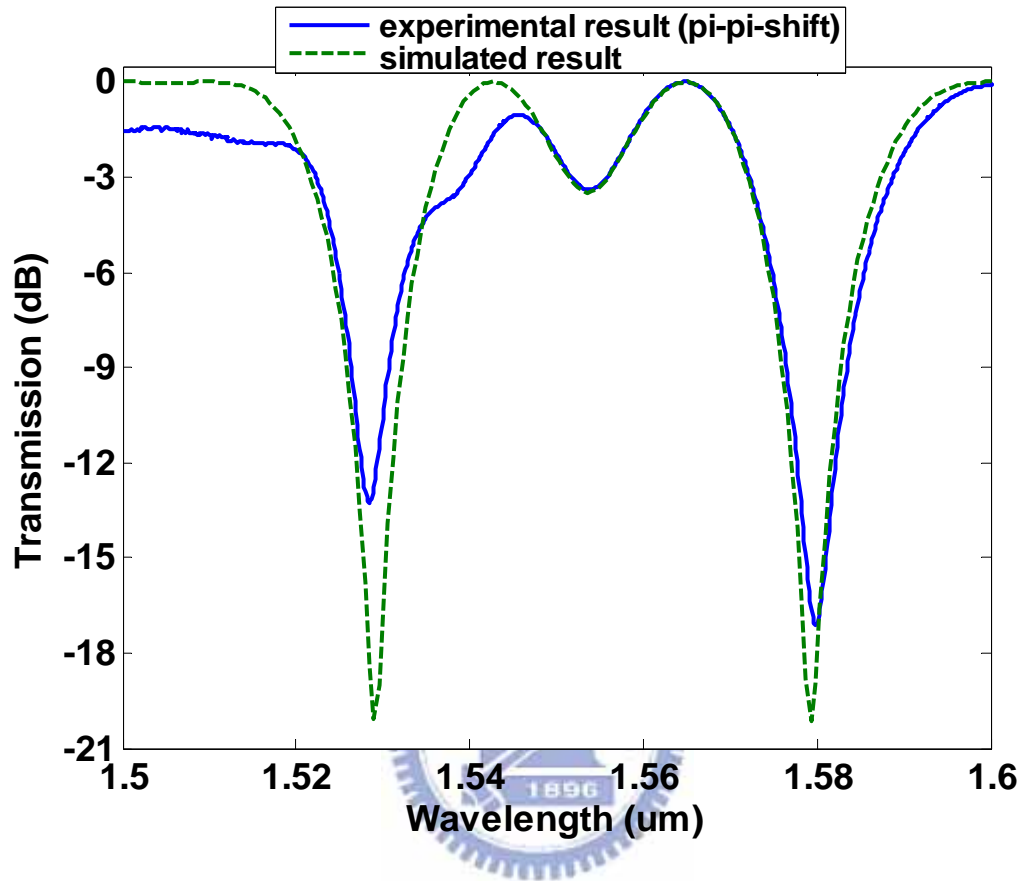


Fig. 3.20 Transmission spectra for double phase-shifted LPG

$$(L_1 = L_2 = L_3 = 15.6\text{mm}, \phi_1 = \phi_2 = \pi)$$

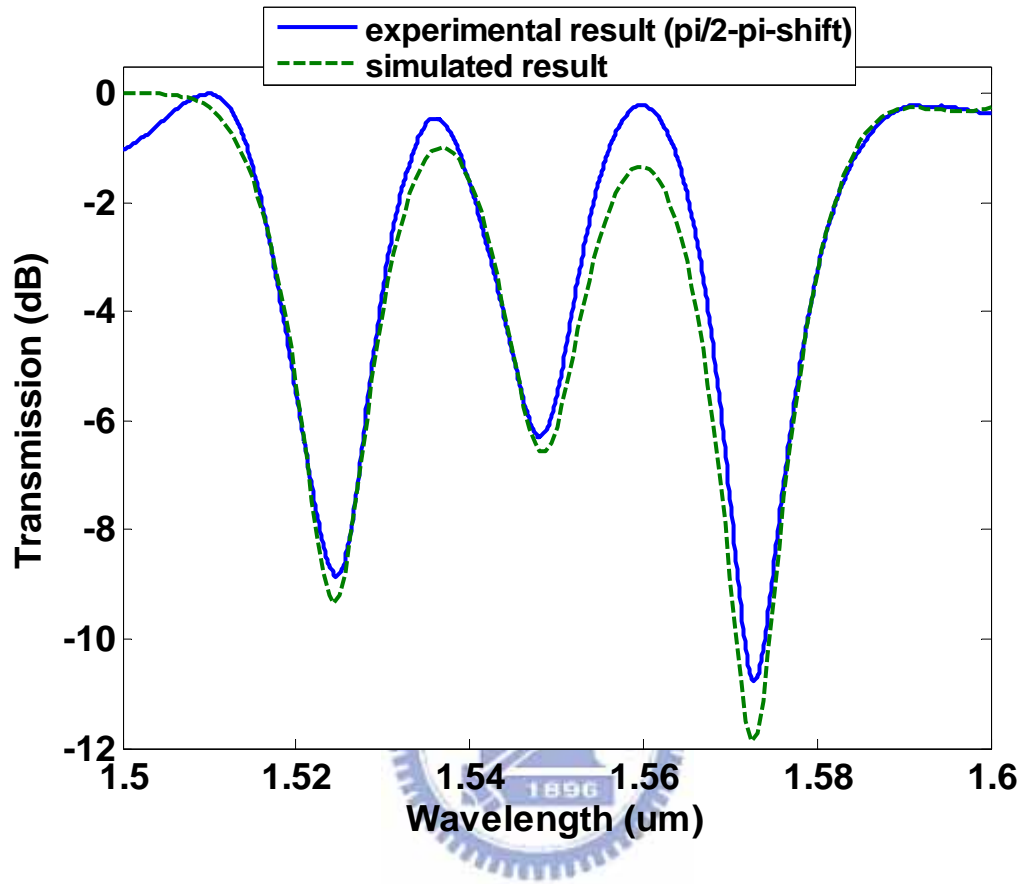


Fig. 3.21 Transmission spectra for double phase-shifted LPG

$$(L_1 = L_2 = L_3 = 15.6\text{mm}, \phi_1 = \pi/2, \phi_2 = \pi)$$

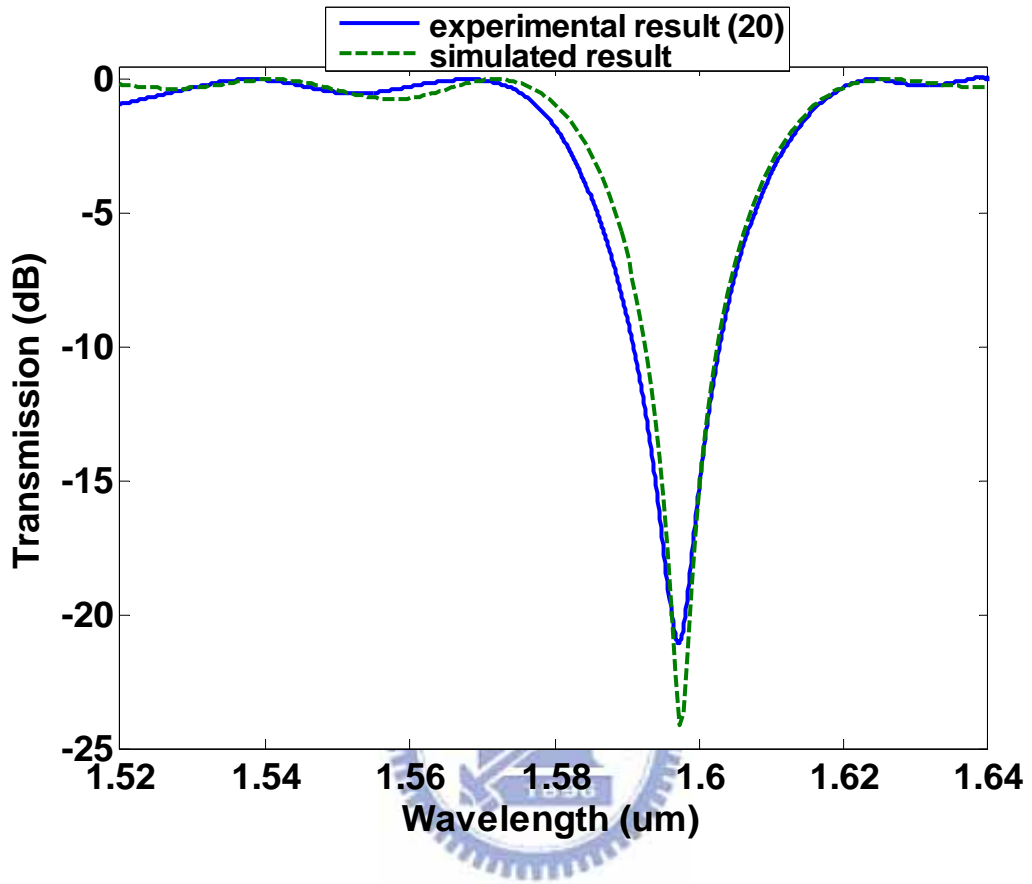


Fig. 3.22 Transmission spectra for multi-phase-shifted LPG

(120 periods, 6 sections, every section 20 periods, 3s)

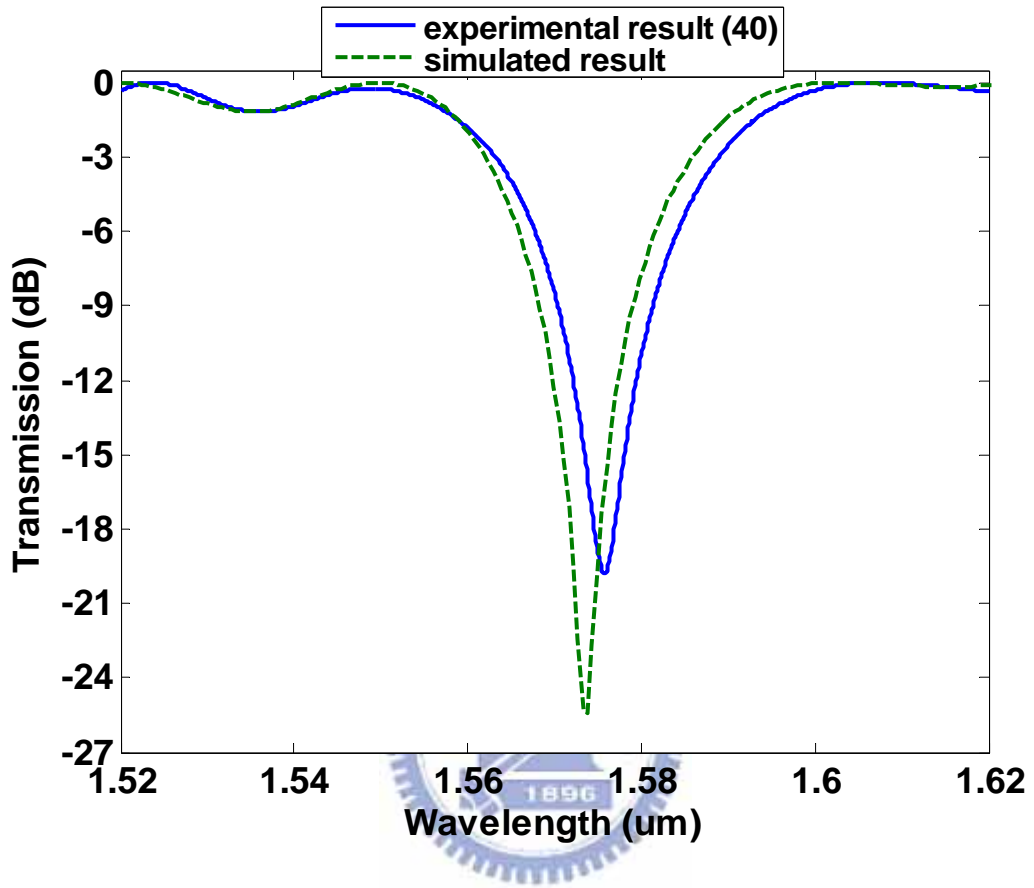


Fig. 3.23 Transmission spectra for multi-phase-shifted LPG

(120 periods, 3 sections, every section 40 periods, 3s)

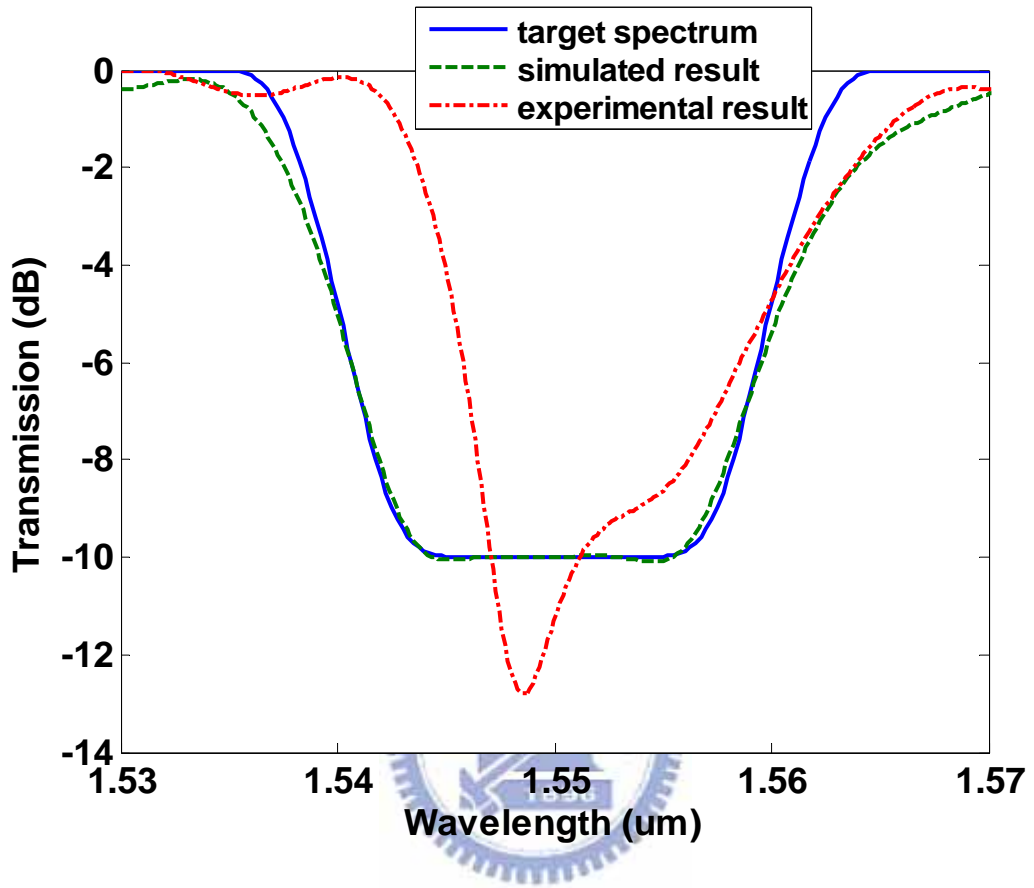
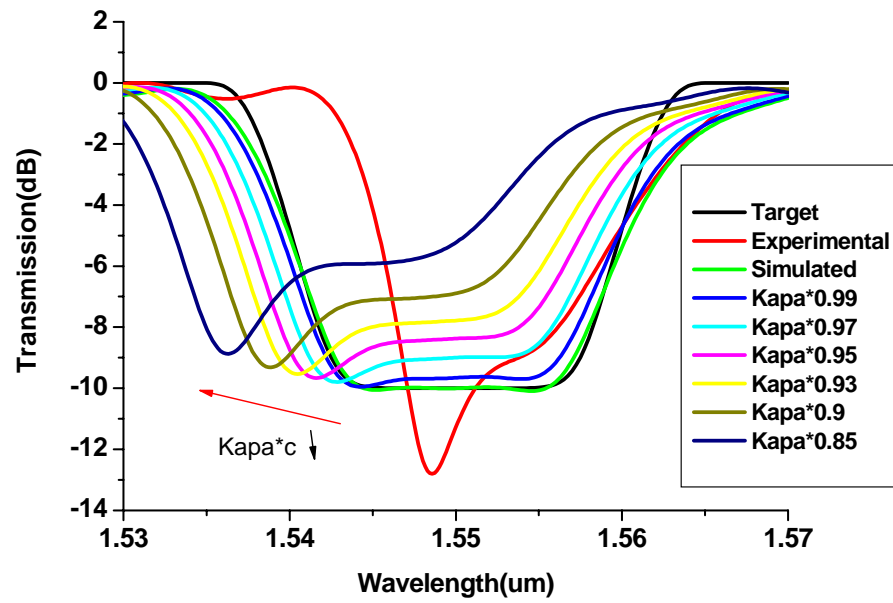
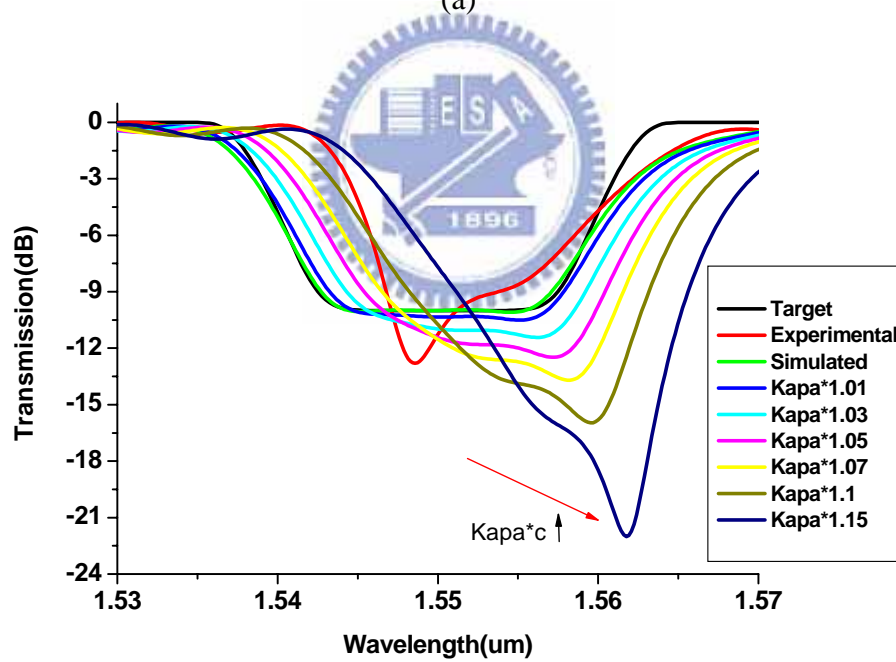


Fig. 3.24 Transmission spectra for the flat-band LPG

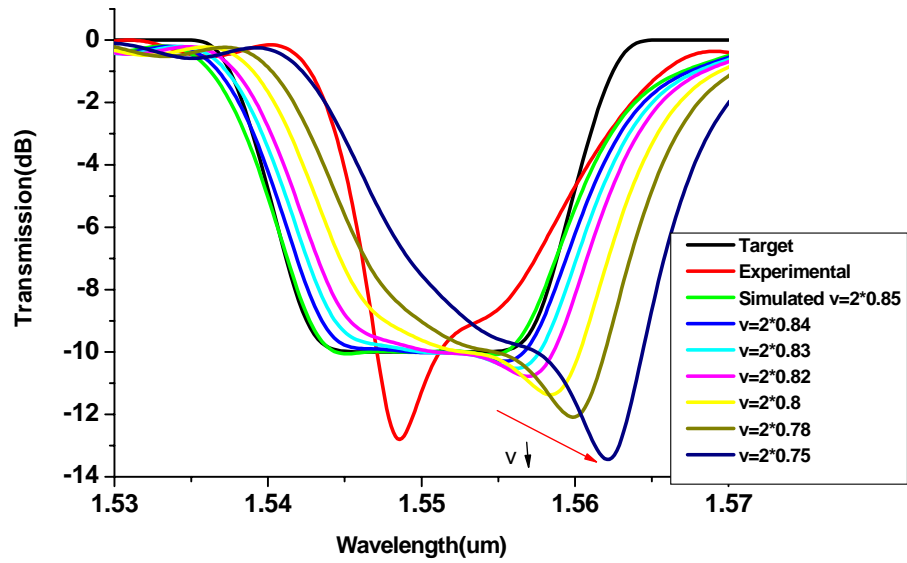


(a)

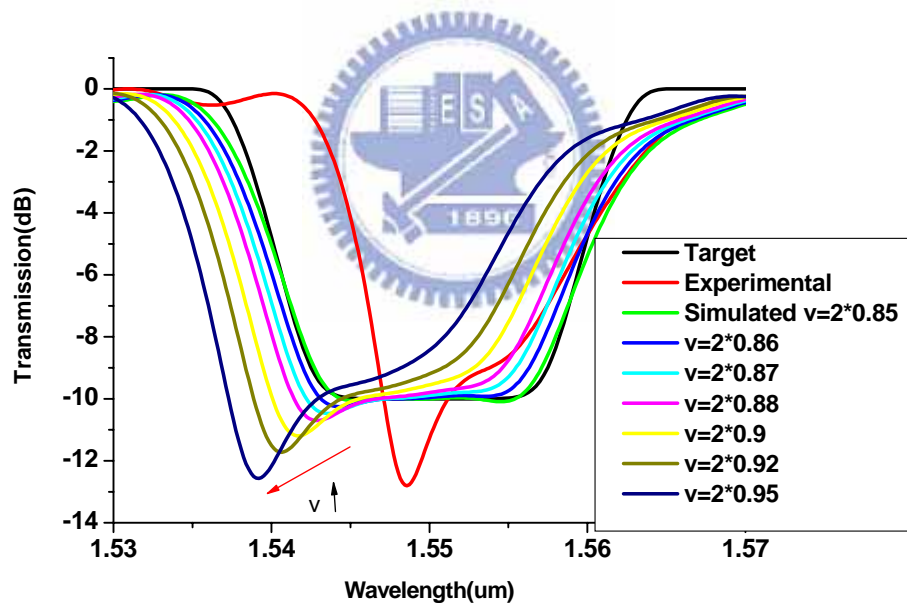


(b)

Fig. 3.25 The simulated spectra with different ratios of the coupling coefficient distribution functions compared to the original one. (a)The ratio is less than one. (b)The ratio is larger than one.



(a)



(b)

Fig. 3.26 The simulated spectra at different fringe visibility of index change compared to the original one. (a) The fringe visibility of index change is less than the simulated one; (b) larger than the simulated one.

Chapter 4. Conclusion and Future Work

4.1 Conclusion

In this thesis, we have designed and fabricated multiple phase-shifted long-period fiber gratings (LPGs). We modulated the refractive index of the fiber core periodically with the point-by-point UV sequential writing method. Considering the values of the induced refractive index change and the beam size, we chose the coupling cladding mode LP₀₈ and the grating period of 260 nm as the main working regime. We fabricated a variety of uniform LPGs with different exposure times to determine the induced refractive index changes. Together with the coupled-mode theory, we got the calibrated results for the fiber core refractive index change versus wavelength and the modulated refractive index change versus the exposure time. After the calibration, we used the single phase-shifted, double phase-shifted and multi-phase-shifted LPGs to check our calibrated results. Then we used the verified parameters and the Evolutionary Programming (EP) algorithm to design the optimal coupling coefficient distribution function for flat-band LPGs. By controlling the exposure time and the phase shift between each uniform LPGs, in principle the flat-band LPGs can be constructed by the sequential point-by-point writing method.

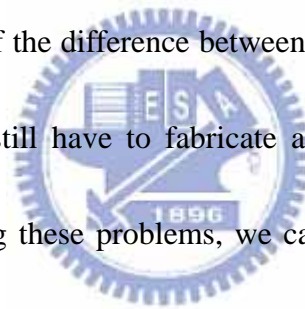
When comparing our preliminary experimental result of the flat-band LPG with the simulated one, they are quite different at the first sight. We found that this is mainly caused by

the difference between the fabricated and simulated coupling coefficient distribution functions.

From our analysis, we also identified that the main error should be caused by the difference in the fringe visibility of the index change between the fabricated coupling coefficient distribution function and the simulated one.

4.2 Future Work

The final goal of our study is to fabricate flat-band LPGs in order to use them as filters or mode converters in optical communication. To achieve this goal, there are still some problems remained to be solved. Because of the difference between the simulated and the experimental results as explained before, we still have to fabricate a new flat-band LPG to justify our design and analysis. After solving these problems, we can then use our verified design and fabrication capability to fabricate more complicated LPG devices for different applications.



References

- [1] K. O. Hill, Y. Fujii, D. C. Johnsen, and B. S. Kawasaki, "Photosensitivity in optical fiber waveguides: Application to reflection filter fabrication," *Appl. Phys. Lett.* Vol. 32, pp. 647-649, 1978.
- [2] G. Meltz, W. W. Morey, and W. H. Glenn, "Formation of Bragg gratings in optical fibers by a transverse holographic method," *Opt. Lett.*, Vol. 14, pp. 823-825, 1989.
- [3] K. O. Hill, B. Malo, F. Bilodeau, D. C. Johnson, and J. Albert, "Bragg gratings fabricated in monomode photosensitive optical fiber by UV exposure through a phase mask," *Appl. Phys. Lett.*, Vol. 62, pp. 1035-1037, 1993.
- [4] J. Albert, K. O. Hill, B. Malo, S. Theriault, F. Bilodeau, D. C. Johnson, and L. E. Erickson, "Apodisation of the spectral response of fiber Bragg gratings using a phase mask with variable diffraction efficiency," *Electron. Lett.*, Vol. 31, pp. 222-223, 1995.
- [5] W. H. Loh, M. J. Cole, M. N. Zervas, S. Barcelos, and R. I. Laming, "Complex grating structures with uniform phase masks based on the moving-scanning beam technique," *Opt. Lett.* Vol. 20, pp. 2051-2053, 1995.
- [6] J. B. Jensen, M. Plougmann, H.-J. Deyerl, P. Varming, J. Hubner, and M. Kristensen, "Polarization control method for ultraviolet writing of advanced Bragg gratings," *Opt. Lett.*, Vol. 27, pp. 1004-1006, 2002.

- [7] A. Asseh, H. Storoy, B. E. Sahlgren, S. Sandgren, and R. Stubbe, "A writing technique for long fiber Bragg gratings with complex reflectivity profiles," *J. Lightwave Tech.*, Vol. 15, pp. 1419-1423, 1997.
- [8] I. Petermann, B. Sahlgren, S. Helmfrid, A. T. Friberg, and P.-Y. Fonjallaz, "Fabrication of advanced fiber Bragg gratings by use of sequential writing with a continuous-wave ultraviolet laser source," *Appl. Opt.*, Vol. 41, pp. 1051-1056, 2002.
- [9] T. Erdogan, "Fiber grating spectra," *J. Lightwave Tech.*, Vol. 15, pp. 1277-1294, 1997.
- [10] G.-W. Chern and L. A. Wang, "Analysis and design of almost-periodic vertical-grating-assisted codirectional coupler filters with nonuniform duty ratios," *Appl. Opt.*, Vol. 39, pp. 4926-4937, 2000.
- [11] G. H. Song, "Toward the ideal codirectional Bragg filter with an acoustooptic-filter design," *J. Lightwave Tech.*, Vol. 13, pp. 470-480, 1995.
- [12] R. Feced, M. N. Zervas, and M. A. Muriel, "An efficient inverse scattering algorithm for the design of nonuniform fiber Bragg gratings," *IEEE J. Quantum Electron.*, Vol. 35, pp. 1105-1115, 1999.
- [13] L. Poladian, "Simple grating synthesis algorithm," *Opt. Lett.*, Vol. 25, pp. 787-789, 2000.
- [14] J. Skaar, L. Wang, and T. Erdogan, "On the synthesis of fiber Bragg gratings by layer peeling," *IEEE J. Quantum Electron.*, Vol. 37, pp. 165-173, 2001.
- [15] J. Skaar and K. M. Risvik, "A genetic algorithm for the inverse problem in synthesis of

- fiber gratings,” J. Lightwave Tech., Vol. 16, pp. 1928-1932, 1998.
- [16] Thomas Back, “Evolutionary algorithms in theory and practice,” Oxford, New York, 1996.
- [17] Cheng-Ling Lee and Yinchieh Lai, “Evolutionary programming synthesis of optimal long-period fiber gratings filters for EDFA gain flattening,” IEEE Photonics Technology Letters, Vol. 14, No. 11, pp. 1557-1559, Nov. 2002.
- [18] Ashish M. Vengsarkar, Paul J. Lemaire, Justin B. Judkins, Vikram Bhatia, Turan Erdogan, and John E. Sipe, “Long-period fiber gratings as band-rejection filters,” J. Lightwave Tech., Vol. 14, No.1, pp. 58-65, Jan. 1996.
- [19] Xuewen Shu, Tom Allsop, Bashir Gwandu, Lin Zhang and Ian Bennion, “High-temperature sensitivity of long-period gratings in B-Ge codoped fiber,” IEEE Photonics Technology Letters, Vol. 13, No. 8, pp. 818-820, Aug. 2001.
- [20] Siddharth Ramachandran, Zhiyong Wang, and Man Yan, “Bandwidth control of long-period grating-based mode converters in few-mode fibers,” Optical letters, Vol. 27, No. 9, pp. 698-700, May 2002.
- [21] Paul F. Wysocki, Justin B. Judkins, Rolando P. Espindola, Matthew Andrejco and Ashish M. Vengsarkar, “Broad-band Erbium-doped fiber amplifier flattened beyond 40 nm using long-period grating filter,” IEEE Photonics Technology Letters, Vol. 9, No. 10, pp. 1343-1345, Oct. 1997.

[22] J. Zhang, P. Shum, S. Y. Li, N. Q. Ngo, X. P. Cheng, and J. H. Ng, "Design and fabrication of flat-band long-period grating," IEEE Photonics Technology Letters, Vol. 15, No. 11, pp. 1558-1560, Nov. 2003.

